

**FINITE STATE MACHINE MODELING OF HUMAN BRAIN RESTING STATE
TRANSITIONS**

by

MASOUMEH GOUDARZI

A thesis submitted to the
Department of Computer Science
in conformity with the requirements for
the degree of Master of Science

Bishop's University
Canada

August 2024

© Masoumeh Goudarzi, 2024
Released under a [CC BY-SA 4.0 License](#)

Abstract

In recent years fMRI has become a pivotal tool in neuroimaging, providing insights into brain activity by detecting changes associated with blood flow. At the same time, the field has also dealt with uncertainty related to many known and unknown effects of artifact in fMRI data and accurately separating signal from noise and identifying meaningful patterns of brain activity. Traditional single-echo fMRI methods are often limited by their susceptibility to artifacts and physiological noise. This research uses multi-echo fMRI acquisitions in conjunction with a multi-echo independent component analysis (ME-ICA) approach has been introduced as a means to automatically distinguish functionally related BOLD signal components from signal artifacts, with significant gains in sensitivity, statistical power, and specificity. Moreover, the research explores the application of Finite State Machines (FSM) and graph theory to multi-echo fMRI modeling of human brain resting state transitions. The findings reveal that while all brain networks are functional connectivity, the connectivity between the Default Mode Network and Motor Network, as well as between the Motor Network and Gray Matter Network 1, are particularly notable and highest. The results advance our understanding of neural connectivity and brain dynamics, offering insights into cognitive and behavioral functions and contributing to the development of targeted interventions and neuroimaging techniques.

Acknowledgments

I would like to extend my deepest gratitude to my supervisor, Dr. Madjid Allili and my co-supervisor Dr. Russell Butler, for their exceptional guidance, steadfast support, and invaluable expertise throughout my MSc project. Their consistent encouragement, thoughtful insights, and constructive feedback have been crucial in shaping the trajectory and enhancing the quality of this thesis. Also, their dedication to my academic growth has been both inspiring and instrumental.

I am profoundly thankful for the unwavering support and encouragement from my husband, son, and parents. Their motivation, patience, and understanding have been indispensable throughout this demanding journey, and their belief in my abilities has provided me with the strength to persevere.

I also wish to acknowledge the faculty and staff at Bishop's University for creating a supportive and enriching academic environment. Their provision of essential resources and their commitment to fostering a culture of learning and inquiry have greatly contributed to my academic experience.

Contents

1	Introduction	1
1.1	Background	1
1.2	Problem Statement	2
1.3	Research Objectives	2
2	Literature Review	3
2.1	Functional Magnetic Resonance Imaging(fMRI)	3
2.1.1	Overview of fMRI principles and the BOLD signal:	3
2.2	Multi-echo fMRI (ME-fMRI)	4
2.2.1	Multi-echo data acquired at 7 T with 2.5 mm isotropic resolution	7
2.2.2	illustrates a representative case of using T2* maps	9
2.2.3	Combination of echo images from a multi-echo fMRI	10
2.3	Classifying statistical components of fMRI datasets	11
2.4	ME-ICA for fMRI Analysis	15
2.4.1	Practical Approaches and Techniques for Denoising fMRI Data	16
2.5	Graph Theory in Neuroimaging	21
2.5.1	Fundamentals of Graph Theory	21
2.5.2	Using Graph Theory to Quantify Resting-State Connectivity	22
3	Methodology	23
3.1	Dataset	23
3.2	Multi-Echo denoising	24
3.2.1	Explanation of Denoising Methods	24
3.3	Identifying Resting-State Networks (RSNs) Using Independent Component Analysis(ICA)	25
3.3.1	Component Map of resting-state networks	26
3.3.2	Creating Spatial Masks and Isolating Time Series	30
3.4	Finite state machine construction	41

3.4.1 Mathematical Equations to Calculate Transitions and Their Probabilities	42
3.5 Graph construction	43
4 Experimental Results	45
4.1 Average time the brain spent	45
4.1.1 Average time the brain spent in each network and each subject	45
4.1.2 Average Time Spent Across All Subjects	47
4.2 Finite State Machine (FSM) in graph form	48
4.2.1 Directed Graph for Each Subject	48
4.2.2 Average Directed Graph Across All Subject	55
4.3 Average transition probabilities matrix	57
5 Discussion	59
5.1 Implications of Findings	59
5.1.1 Functional connectivity of network component across all subjects	59
5.1.2 Inter-Subject Variability of Functional connectivity	60
5.1.3 Implications for neuroscience	62
5.2 Limitations and Challenges	63
5.3 Future Research Directions	64
6 Conclusion	66
Bibliography	67

List of Abbreviations

Abbreviation	Definition
BOLD	Blood Oxygen Level Dependent
CSF	Cerebrospinal Fluid
DMN	Default Mode Network
EEG	Electroencephalography
fMRI	Functional Magnetic Resonance Imaging
FSM	Finite State Machine
FSL	FMRIB Software Library
GLM	General Linear Modeling
ICA	Independent Component Analysis
ICs	Independent Components
MEG	Magnetoencephalography
ME-ICA	Multi-Echo Independent Component Analysis
ME-fMRI	Multi-Echo Functional Magnetic Resonance Imaging
MELODIC	Multivariate Exploratory Linear Optimized Decomposition into Independent Components
MESMS	Multi-Echo Simultaneous Multi-Slice
OC	Optimal Combination
RSNs	Resting-State Networks
SNR	Signal-to-Noise Ratio
SPEP	Spiral and Echo Planar
TEs	Echo Times
TR	Repetition Time

List of Figures

2.1	figure 1. Multi-echo fMRI images from 3 T and 7 T	5
2.2	figure 2. Multi-echo data acquired at 7 T	7
2.3	figure 3. T2* maps for anatomical-functional co-registration	9
2.4	figure 4. Combination of echo images from a multi-echo fMRI experiment	10
2.5	figure 5. Multi-echo independent components analysis (ME-ICA) . .	12
2.6	figure 6. Pipeline of component and time series outputs from ME-ICA	18
2.7	figure 7. Cortical dynamics captured in high- κ time series	19
2.8	figure 8. Detection of sigmoidal BOLD effect after separating BOLD from non-BOLD signals	20
3.9	figure 9. Default Mode Network	27
3.10	figure 10. Motor Network	27
3.11	figure 11. Visual Network	28
3.12	figure 12. Right Executive Network	28
3.13	figure 13. Left Executive Network	29
3.14	figure 14. Gray Matter Network 1	29
3.15	figure 15. Gray Matter Network 2	30
3.16	Figure 16. Brain Network Component Mask for Subject 1	31
3.17	Figure 17. Brain Network Component Mask for Subject 2	32
3.18	Figure 18. Brain Network Component Mask for Subject 3	32
3.19	Figure 19. Brain Network Component Mask for Subject 4	33
3.20	Figure 20. Brain Network Component Mask for Subject 5	33
3.21	Figure 21. Brain Network Component Mask for Subject 6	34
3.22	Figure 22. Time series for all network components of Subject 1	35
3.23	Figure 23. Time series for all network components of Subject 2	36
3.24	Figure 24. Time series for all network components of Subject 3	37
3.25	Figure 25. Time series for all network components of Subject 4	38
3.26	Figure 26. Time series for all network components of Subject 5	39
3.27	Figure 27. Time series for all network components of Subject 6	40
4.28	Figure 28. Average Time Spent in Each Brain Network for Each Subject	46
4.29	Figure 29. Average Time Spent Across All Subjects	47
4.30	Figure 30. Finite State Machine of network component of Subject 1 .	49
4.31	Figure 31. Finite State Machine of network component of Subject 2 .	50

4.32	Figure 32. Finite State Machine of network component of Subject 3	51
4.33	Figure 33. Finite State Machine of network component of Subject 4	52
4.34	Figure 34. Finite State Machine of network component of Subject 5	53
4.35	Figure 35. Finite State Machine of network component of Subject 6	54
4.36	Figure 36. Finite State Machine of network component across all subjects	55
4.37	Figure 37. Average transition probabilities matrix of network component across all subjects	57

Chapter 1

Introduction

1.1 Background

Functional magnetic resonance imaging (fMRI) has become a pivotal tool in neuroimaging, providing insights into brain activity by detecting changes associated with blood flow [7]. The recent introduction of simultaneous multi-slice (SMS) acquisitions has enabled the acquisition of blood oxygen level dependent (BOLD) functional magnetic resonance imaging (fMRI) data with significantly higher temporal sampling rates. In a parallel development, the use of multi-echo fMRI acquisitions in conjunction with a multi-echo independent component analysis (ME-ICA) approach has been introduced as a means to automatically distinguish functionally related BOLD signal components from signal artifacts, with significant gains in sensitivity, statistical power, and specificity [26]. Also, ME-ICA identifies significantly more BOLD-like components in the MESMS data as compared to data acquired with a conventional multi-echo single-slice acquisition.

Finite State Machines (FSMs) offer a powerful framework for modeling brain state transitions, capturing the dynamic nature of neural activity. FSMs can effectively describe how the brain transitions between different states based on stimuli or internal processes, providing insights into the underlying mechanisms of brain function. By applying FSMs to neuroimaging data, researchers can map out the sequence of brain states and predict future states, enhancing our understanding of cognitive processes and neurological disorders [30, 39]. This approach has the potential to reveal patterns in brain activity that are not evident through traditional analysis methods, offering a new dimension of analysis in neuroscientific research.

This research explores the application of graph theory to multi-echo fMRI data analyzed with ME-ICA, specifically focusing on the complex five-dimensional datasets that include dimensions of space (x, y, z), time, and echo.

1.2 Problem Statement

The primary challenge in fMRI data analysis lies in accurately separating signal from noise and identifying meaningful patterns of brain activity. Traditional single-echo fMRI methods are often limited by their susceptibility to artifacts and physiological noise. This research aims to model the brain using a Finite State Machine (FSM) to produce insights into how the brain transitions between different states. Applying graph theory to multi-echo fMRI data serves this goal by potentially offering more robust and precise analysis tools for neuroscientific research [7].

1.3 Research Objectives

The research aims to achieve the following objectives:

1. To investigate the efficacy of graph theory in analyzing multi-echo fMRI. This involves applying graph theoretical methods to identify and model the dynamic transitions between different brain states. By using a Finite State Machine (FSM) to represent these transitions, the study seeks to provide deeper insights into the functional connectivity and temporal dynamics of the brain. The goal is to demonstrate that graph theory can enhance the precision and robustness of fMRI data analysis, overcoming limitations associated with traditional methods.
2. creating a finite state machine (FSM) with transition probabilities between ICA component states in order to quantify brain state transitions.

Chapter 2

Literature Review

2.1 Functional Magnetic Resonance Imaging(fMRI)

2.1.1 Overview of fMRI principles and the BOLD signal:

Functional magnetic resonance imaging (fMRI) relies on the Blood Oxygen Level Dependent (BOLD) contrast mechanism, which was first described by Ogawa et al. (1990). The BOLD signal arises from changes in blood oxygenation levels, which affect the magnetic properties of hemoglobin and, consequently, the MRI signal. When neural activity increases in a region, the local blood flow and oxygenation levels change, leading to detectable signal variations in the MRI data. This principle allows researchers to map brain activity non-invasively [25].

Blood oxygenation level dependent (BOLD) functional MRI (fMRI) is widely used to study brain activity based on hemodynamic signals [2, 9, 12, 18]. However, recent studies show that fMRI data can be severely affected by artifacts [28]. These artifacts relate to subject head motion, cardiac and respiratory effects, and hardware [19, 21]. Studies on the effects of fMRI artifacts have brought into question many of the compelling findings on brain function based on fMRI, for example, relating to human brain development [17]. fMRI artifacts also reduce the statistical power of fMRI studies and lead to spurious findings, which has been associated with a crisis of confidence in fMRI research [11]. Thus, while in recent years the field of fMRI research has both enjoyed advanced technology and expanded use, it also deals with a deep discomfort related to many known and unknown effects of artifact. Multi-echo (ME)-fMRI aims to enhance the fidelity of fMRI signals by using a physically driven approach to determine whether the signals originate from BOLD contrast or artifacts. This technique can be further optimized by combining ME methods with emerging multi-band acceleration techniques, resulting in fMRI strategies that offer both high resolution and fidelity. Overall, ME-fMRI involves only a few relatively minor changes from standard fMRI acquisition techniques, yet it enables analyses that significantly improve the quality of fMRI data [22].

To date, the challenges in controlling fMRI artifacts have been met with generic time series signal processing methods such as regression and frequency-restricting bandpass filters [33]. Head motion artifacts, modeled from shifts in brain images over time, are regressed out of fMRI time series. Recordings of physiology during MRI are used to model cardiac and respiratory artifact regressors [19]. Spontaneous activity is bandpass filtered to retain a narrow range of frequencies in order to exclude hardware-related signal drifts and high-frequency noise [13]. Time series models of noise and usually their temporal derivatives are linearly regressed out of data. Despite the significant reduction in information in data after applying these steps, it is now clear that much artifact remains. Of late, simple deletion of volumes from fMRI datasets has been suggested [28]. This altogether means that artifact signals are not characterized well enough by modeling artifact time courses and regressing them out of data. This reality also suggests that artifacts are themselves various and complex and may interact in unpredictable ways. At the heart of the issue, however, is that standard fMRI approaches do not have a strong and general ground truth to precisely relate signals to biophysical signal mechanisms versus artifacts. Given information on how signals scale across the echo images of an ME-fMRI experiment, however, valuable insight on the origins of fMRI signals in BOLD contrast or artifact can be gained.

2.2 Multi-echo fMRI (ME-fMRI)

After excitation, standard fMRI uses 2-D echo planar imaging to acquire slice images at a single TE, one slice at a time. At 3 T, this TE is usually 30 ms. ME-fMRI uses a slightly different approach. After a normal excitation pulse, a slice image is acquired at the earliest TE possible. Without exciting again, readout of another image of the same slice is then acquired immediately afterward, at a longer TE, and so forth up to the desired number of images and TEs. This happens for each slice of the brain volume. Using this approach, in most cases, there is no cost for acquiring the early TE, since standard fMRI pulse sequences are idle during the early period after excitation. Acquiring extra images after the ‘standard’ intermediate TE is the main cost. The important benefit is that the $T2^*$ signal decay can be modeled for each voxel. This information can be used to relate signals to their generative physical processes and can help in mitigating artifacts of many kinds.

Different voxels have different $T2^*$ decay depending on tissue properties and variation of the local magnetic field. These properties can be parameterized based on an ME experiment. ME images can be acquired using 3 T and 7 T MRI (Fig. 1).

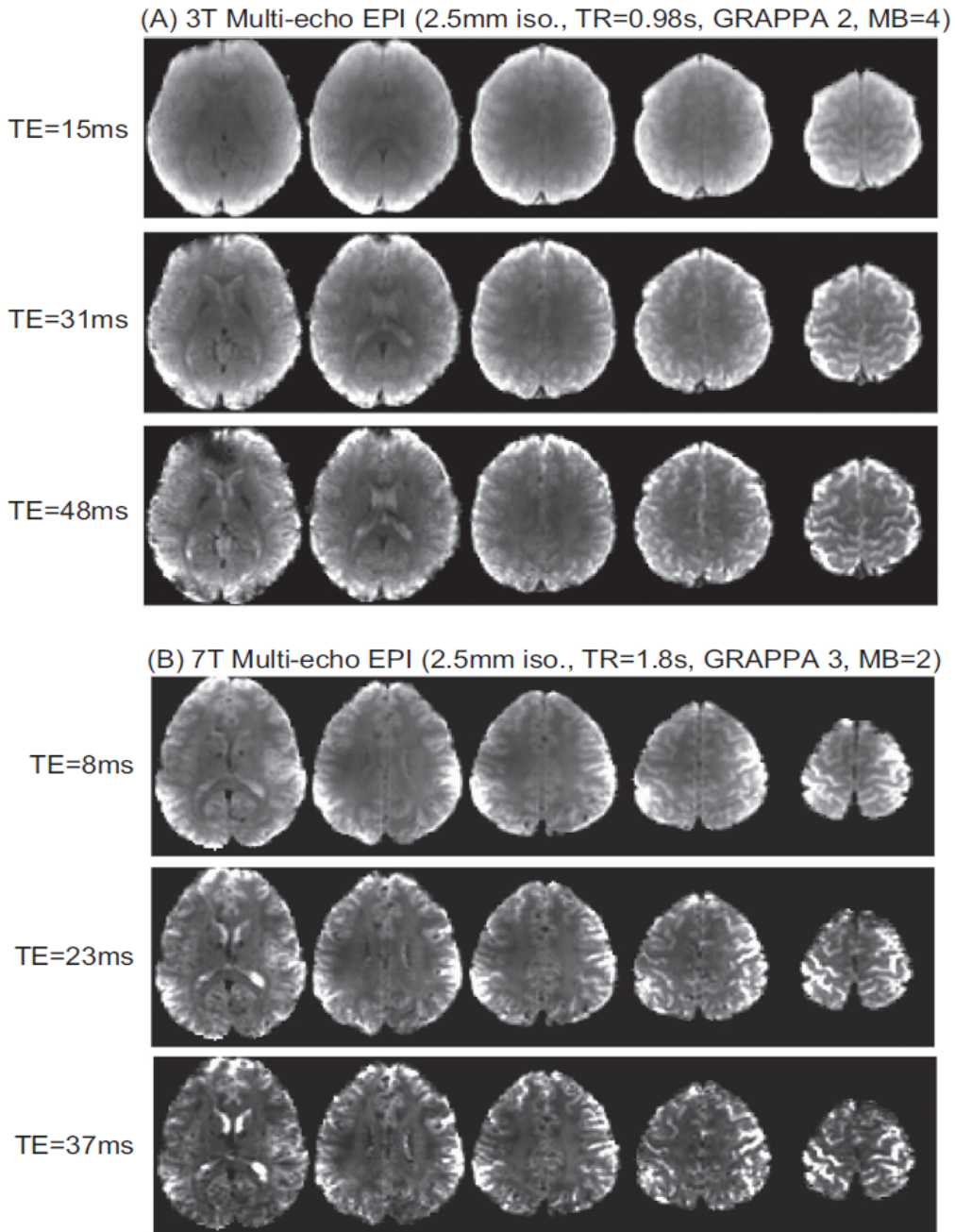


Figure 2.1: Multi-echo fMRI images from 3 T and 7 T. (A) 3 T multi-echo images with in plane and multi-band acceleration with 2.5 mm isotropic resolution and < 1 s TR. (B) 7 T multi-echo images with GRAPPA factor 3 and 2.5 mm isotropic resolution, no multiband acceleration, giving TR=2.5 s [23].

Multi-echo fMRI (ME-fMRI) enhances the quality of BOLD signals by acquiring multiple echoes at different echo times (TEs) within each repetition time (TR). This method significantly improves the separation of BOLD and non-BOLD components, which is critical for accurate fMRI analyses. The approach leverages the differential decay characteristics of these components across multiple echo times, which allows for better differentiation between true neural signals and various artifacts, such as those caused by physiological fluctuations, head motion, and scanner-related noise [23].

ME-fMRI provides increased sensitivity and specificity in fMRI studies by utilizing the additional information obtained from multiple echoes. This technique is particularly effective in reducing the impact of artifacts on fMRI data, leading to cleaner and more reliable results [26].

By capturing the signal decay at different echo times, ME-fMRI enables a more precise identification of the BOLD signal, enhancing the overall quality of the fMRI data [23].

One of the key benefits of ME-fMRI is its ability to improve data quality by providing a clearer separation of signal and noise. This results in higher fidelity BOLD signals, which are crucial for accurate brain mapping and functional connectivity studies. Additionally, ME-fMRI's enhanced sensitivity and specificity contribute to more robust findings in fMRI research, as it allows for the detection of subtle neural activations that might be missed with traditional single-echo fMRI methods [26].

2.2.1 Multi-echo data acquired at 7 T with 2.5 mm isotropic resolution

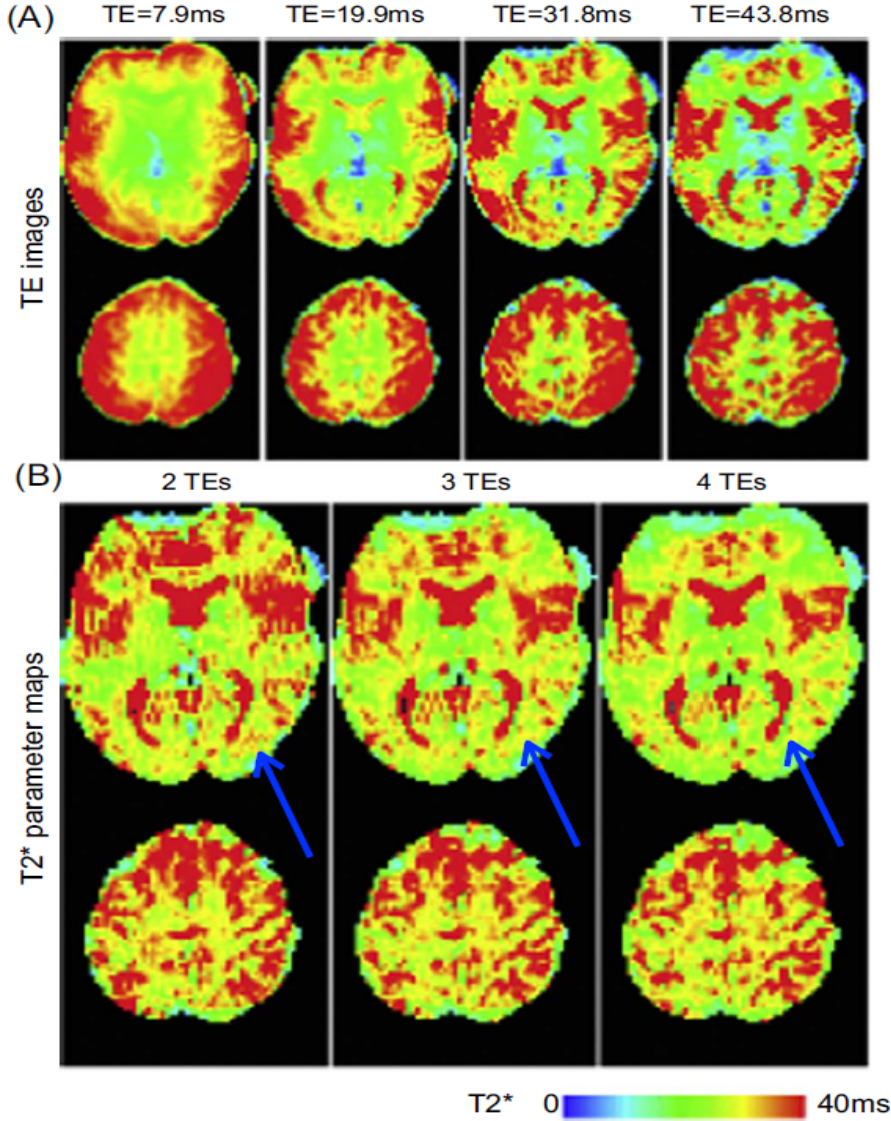


Figure 2.2: For multi-echo data acquired at 7 T with 2.5 mm isotropic resolution, (A) TE images in arbitrary units, colorized. Tissue contrast changes with TE, but CSF or gray matter compartments are unclear. (B) Calculation of $T2^*$ maps using 2 to 4 echo images. Using just 2 TE images to generate a $T2^*$ map is informative of CSF localization, emphasized in ventricles (top pane) and in subarachnoid space (bottom pane). However, checkering artifact is present. As more TEs are used for estimating $T2^*$ maps, the influence of artifact on $T2^*$ estimates decreases. The precision of anatomical localization of $T2^*$ values also increases when using more TE images for parameter estimates (arrows) [26].

In part A, TE images in arbitrary units, colorized. Tissue contrast changes with TE, but cerebrospinal fluid (CSF) or gray matter compartments are unclear.

part B shows Calculation of $T2^*$ maps using 2 to 4 echo images. Using just 2 TE images to generate a $T2^*$ map is informative of CSF localization, emphasized in ventricles (top pane) and in subarachnoid space (bottom pane). However, checkerboard artifact is present. As more TEs are used for estimating $T2^*$ maps, the influence of artifacts on $T2^*$ estimates decrease. The precision of anatomical localization of $T2^*$ values also increase when using more TE images for parameter estimates (arrows) [26].

2.2.2 illustrates a representative case of using T2* maps

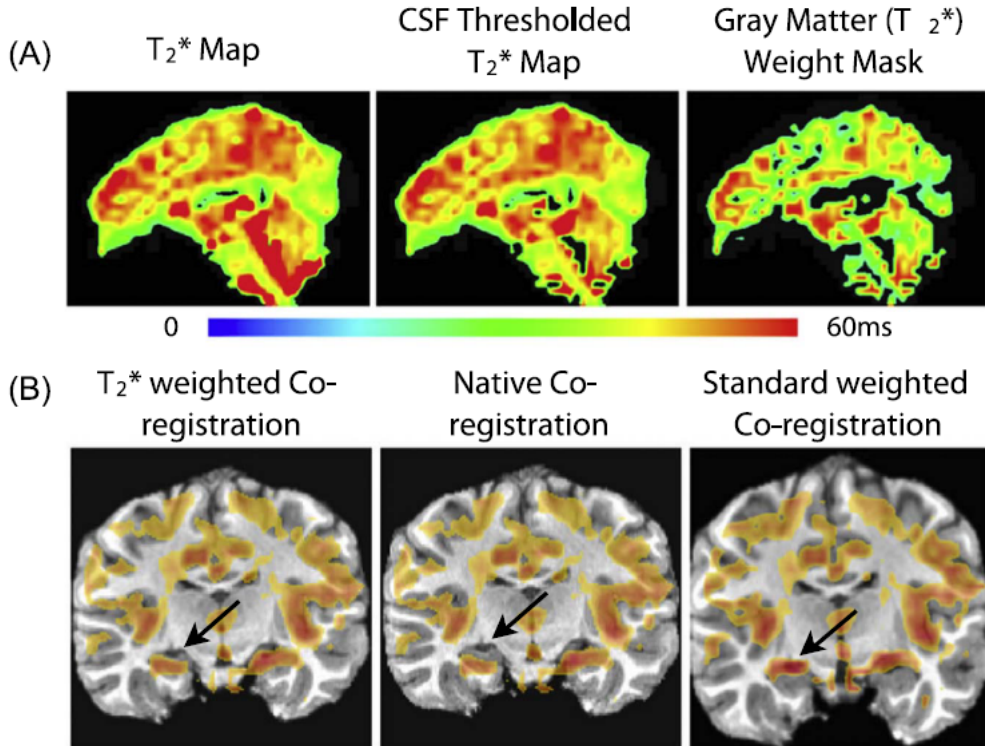


Figure 2.3: A representative case of using T2* maps to drive anatomical-functional co-registration. (A) T2* map generated from multi-echo fMRI data. The T2* map is thresholded to mask out CSF, by modeling CSF as having twice the T2* of gray matter. This masked T2* map is segmented, to generate a T2* weight mask for driving anatomical-functional segmentation. (B) T2* weighted co-registration uses local Pearson correlation to estimate an affine warp. The weight maps show high intensity in gray matter, including hippocampus. Native co-registration (i.e., rigid-body) mis-registers subcortical areas. Standard affine warp based on global estimate over scales the anatomical image [23].

The first image, part A, shows a T2* map generated from multi-echo fMRI data. This map visualizes the variation in T2* values across the brain, providing a detailed view of tissue properties. The second image presents the T2* map thresholded to mask out cerebrospinal fluid (CSF), by modeling CSF as having twice the T2* of gray matter. This step helps in enhancing the contrast between gray matter and other tissues. The third image displays a gray matter (T2*) weight mask, segmented

from the thresholded T2* map. This mask is used to generate a T2* weight map for driving anatomical-functional segmentation.

The next set of images, part B, shows T2* weighted coregistration, which uses local Pearson correlation to estimate an affine warp. The weight maps in this method show high intensity in gray matter, including the hippocampus. The second image presents native coregistration, which is a rigid-body method that often mis-registers subcortical areas. The third image illustrates standard weighted coregistration, where a standard affine warp based on a global estimate often overscales the anatomical image.

Finally, Figure 3 demonstrates the process and benefits of using T2* maps for improving the anatomical-functional co-registration in fMRI studies. The T2* maps generated from multi-echo fMRI data provide a more accurate representation of tissue properties, enhancing the segmentation and co-registration processes [23].

2.2.3 Combination of echo images from a multi-echo fMRI

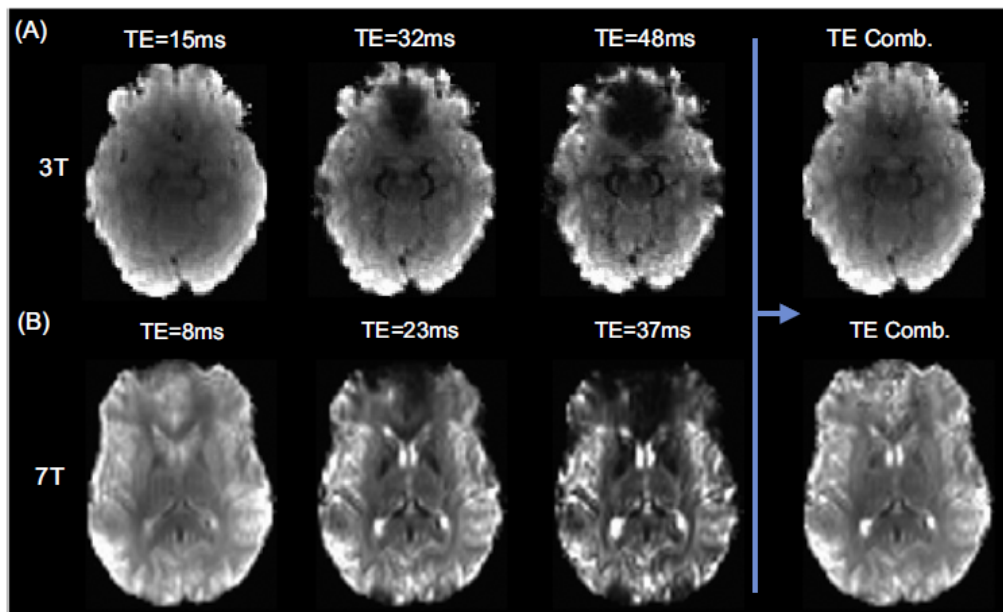


Figure 2.4: Combination of echo images from a multi-echo fMRI experiment to provide an optimally combined image. This figure demonstrates how multiple echo times (TEs) can be used to enhance image quality by reducing artifacts [22].

The images at the top row (3T) show brain scans at different echo times: TE=15ms, TE=32ms, and TE=48ms. Each image captures different aspects of the brain's signal

decay. The final image in this row labeled "TE Comb." represents the optimally combined image using data from the multiple echo times, which enhances the overall image quality by mitigating artifacts and improving the signal-to-noise ratio.

The images at the bottom row (7T) show brain scans at different echo times: TE=8ms, TE=23ms, and TE=37ms. Similar to the top row, these images capture various details of the brain's signal decay at a higher magnetic field strength (7T). The final image in this row labeled "TE Comb." represents the optimally combined image at 7T, demonstrating improved image quality and reduced artifacts.

The combination of echo images from a multi-echo fMRI experiment helps in creating an optimally combined image. This method addresses signal dropout artifacts that occur due to short T2* in areas of high susceptibility. By weighting the combination towards early TE signals in short T2* areas, the method significantly improves the quality of the final image. The figure illustrates how using multiple echo times and combining them effectively can enhance the fidelity of fMRI data, leading to clearer and more reliable imaging results [22].

2.3 Classifying statistical components of fMRI datasets

TE-dependence and TE-independence models can be utilized to classify signal components in fMRI identified using spatial independent component analysis (ICA) [23]. ICA is an effective method that decomposes fMRI time series data into linearly separable component maps and their corresponding time courses, represented as:

$$X(v, t) = A(v, c) \cdot w(c, t) \quad (\text{Equation 1})$$

where X is a voxel-by-time matrix of time series, A is a voxel-by-component matrix of spatial maps, and w is a component-by-time matrix representing the modulation of maps over time. ICA aims to find component maps that are statistically independent from one another. One metric for estimating independence is negative entropy, used in InfoMax ICA [5]. Another metric is kurtosis, the fourth statistical moment, used in FastICA. This approach is computationally efficient and effective in identifying independent components [5]. Consequently, FastICA is suitable for large datasets, such as those from long-duration, high-temporal-resolution experiments, and is the primary algorithm in the MELODIC tool within the FSL suite [35].

Applying MELODIC ICA to ME-fMRI data results in components that resemble functional networks, such as the default mode network, and artifacts, like pulsation (Fig. 5).

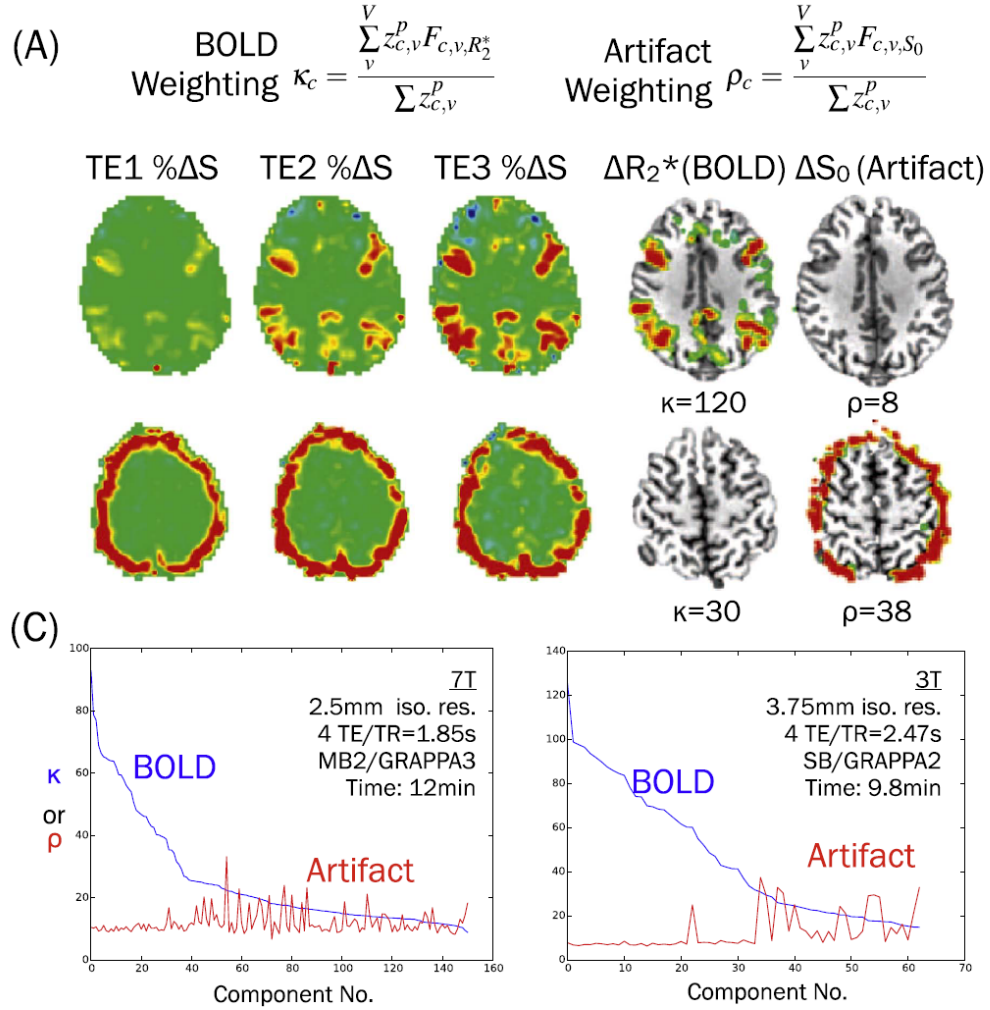


Figure 2.5: Multi-echo independent components analysis (ME-ICA). (A) κ and ρ pseudo-F statistics representing component-level TE-dependence and independence, of BOLD and artifact, respectively. (B) In the first three columns, the percent signal changes across TEs, of network and artifact components in top and bottom rows, respectively. The last two columns show parameter maps from fitting percent signal changes to TE-dependence and TE-independence models, thresholded by goodness of fit FR_2^* and FS_0 , respectively. (C) κ and ρ spectra, for 7 T and 3 T data. [35].

Analyzing the component time series with unit variance against the different voxel time series and TEs showed that network components exhibit statistically significant linear scaling with TE, fitting well to the linear TE-dependence model. Conversely, many artifact components show constant percent signal change with TE. The

significance of the fits can be determined using F-statistics with degrees of freedom ($N_{echo}, 1$), one for the TE-dependence model and another for the TE-independence model, which are numerically comparable.

F-statistics are used to threshold the parameter maps for ΔR_2^* and ΔS_0 . These maps reflect the percent signal change from fitting time series points to either a slope or a constant line, suggesting that TE-dependence and TE-independence model fitting of ICA component amplitudes is a robust method for inferring the physical sources of component signals.

Overall weightings for TE-dependence and TE-independence have been proposed to characterize ICA components in fMRI datasets [23]. Simple averaging of FR2* and FS0 over each component does not effectively differentiate network maps from artifact maps, as most voxels are not significant. Therefore, a weighted average using Z-maps from the ICA mixing matrix fitting is employed. The Z-weighted average of FR2* values is called κ (Fig. 5a), and the same for FS0 values is called ϱ . The Scree plot of κ values for all components is the κ spectrum. Plotting ϱ values in the same order reveals the relative TE-dependence and TE-independence per component.

ICA components in ME-fMRI datasets cluster into two regimes: one with high κ and low ϱ , and the other with low κ and/or high ϱ (Fig. 5c). High κ components include cortical networks with high percent signal change and smaller magnitudes like subcortical components of the putamen. Low κ components include artifacts such as pulsatility, motion, and the sagittal draining vein. These findings indicate that ICA can classify components into network and artifact groups based on TE-dependence and TE-independence, suggesting that multi-echo fMRI data acquisition could be a viable approach for ICA component classification.

These results highlight that ICA, despite being a statistical technique, can identify biophysically specific modulations. Modeling ΔR_2^* and ΔS_0 of components identifies two clear regimes separating networks and artifacts [23]. This framework is termed multi-echo ICA (ME-ICA).

detailed explanations of each network are provided below to elucidate their roles and significance:

- **Default Mode Network (DMN)**

The Default Mode Network (DMN) is a well-researched network in neuroimaging, predominantly active when an individual is at rest and not engaged in external tasks. This network is associated with self-referential thoughts, memory retrieval, and planning for the future. Key regions involved include the medial prefrontal cortex, posterior cingulate cortex, precuneus, and lateral parietal cortex [31].

- **Motor Network**

The Motor Network is integral for the planning, control, and execution of voluntary movements. It encompasses regions such as the primary motor cortex, supplementary motor area, and parts of the parietal lobe. This network is essential for coordinating motor functions and integrating sensory feedback to guide movements [6].

- **Visual Network**

The Visual Network is responsible for processing visual information and includes regions like the primary visual cortex (V1) and other areas within the occipital lobe. This network exhibits synchronous activity even in the absence of visual stimuli, highlighting its role in visual perception and readiness to process visual data [31].

- **Right Executive Network (RExec)**

The Right Executive Network plays a critical role in high-level cognitive functions such as working memory, decision-making, and cognitive control. This network includes regions like the right dorsolateral prefrontal cortex and right posterior parietal cortex, which are pivotal for attention and executive processes [34].

- **Left Executive Network (LExec)**

The Left Executive Network, similar to its right counterpart, is involved in executive functions such as working memory and cognitive control, but is lateralized to the left hemisphere. Key regions include the left dorsolateral prefrontal cortex and left posterior parietal cortex [15].

- **Gray Matter Network 1 (GM1)**

Gray Matter Network 1 (GM1) comprises regions within the gray matter that are involved in a variety of cognitive and sensory processes. This network reflects the general functionality of cortical regions responsible for integrating sensory inputs and executing higher-order cognitive functions [37].

- **Gray Matter Network 2 (GM2)**

Similar to GM1, Gray Matter Network 2 (GM2) consists of various regions within the gray matter involved in different cognitive and sensory functions. It underscores the distributed nature of cortical processing and the integration of information across different brain areas [37].

2.4 ME-ICA for fMRI Analysis

ME-ICA demonstrated how brain network components could be separated from various artifacts without relying on spatial or temporal templates of expected functional effects. Although ME-ICA was initially applied to human resting-state fMRI data from 3T MRI, its broader applicability is apparent. TE-independent component time series can be regressed out of fMRI time series to denoise both task and resting-state activities since both arise from BOLD contrast [24]. This allows for denoising within the same analysis framework, contrasting with the current need for distinct pipelines for standard fMRI data of these paradigms. Consequently, ME-fMRI and ME-ICA could simplify fMRI study workflows while maintaining physical principles.

ME-ICA is applicable to any data with T2* signal fluctuations from BOLD contrast, suggesting potential use in animal fMRI. Animal brain anatomy's lower morphological variability compared to human anatomy makes it harder to distinguish artifacts from signals of interest. Thus, automatically and systematically separating BOLD and non-BOLD signals based on ME data is advantageous for animal fMRI. The ME approach can also be applied to fMRI at different field strengths, such as 7T and 1.5T, which have varying associated artifacts but exhibit the same TE-dependence and TE-independence mechanisms. Furthermore, both multi-band and single-band fMRI can be analyzed using the same pipeline, positioning ME-fMRI and ME-ICA as a general model and processing approach for fMRI time series.

A general fMRI model would not require many assumptions about brain activity or artifact patterns in space or time. It would eliminate the need for conditioning steps like band-pass filtering and spatial smoothing, which are typically applied to remove drift and noise. This is especially beneficial for experiments where maintaining a stable signal baseline is crucial, such as pharmacological fMRI or learning tasks. Current techniques like ASL are often suboptimal due to their complexity and low signal-to-noise ratio [1, 14, 23, 40].

The ME-ICA approach begins with isolating thermal noise, which is neither BOLD signal nor non-BOLD artifact and typically follows Rician or Gaussian-like distributions. This noise's prevalence and distribution are determined by the imaging system [41]. Thermal noise and BOLD can overlap at low maximum sampling frequencies, close to 0.3 Hz or lower, as seen in most fMRI studies to date [14]. Given that most fMRI acquisitions cannot achieve very high sample rates, time series filtering is needed to remove thermal noise, which may also eliminate BOLD signals informative for separating artifacts from networks.

In the ME-ICA framework, the proportion of thermal noise decreases with higher field strength and increases with smaller voxel sizes. This approach effectively separates all data into MR signals and Gaussian noise and then into BOLD and non-BOLD sources using analyses of TE-dependence and TE-independence. ME-ICA

has shown promising results in challenging applications like "resting-state" fMRI of the rat brain using a Bruker 11.7 T preclinical MRI with a four-channel head coil, demonstrating clear brain networks with minimal mixed artifacts [23].

ME-ICA also addresses susceptibility-related dynamic artifacts, which arise from shifts in the magnetic field over time, such as due to chest motion during breathing. These artifacts exhibit mixed T2* and S0 origins and tend to have higher κ values than conventional TE-independent artifacts but lower than functional networks. ME-ICA's ability to manage these artifacts suggests it is a robust method for distinguishing between functional BOLD components and artifacts in fMRI data.

Recent studies have demonstrated ME-ICA's increased sensitivity in task-based fMRI analyses. ME-ICA has outperformed conventional denoising and activation mapping methods in terms of activation extent, magnitude, percent detected trials, and effect size. These findings indicate that the general ME-ICA signal model is a versatile and powerful approach for advanced denoising of both task-based and resting-state fMRI data [20].

In summary, ME-ICA provides a general signal model and processing approach for fMRI time series by effectively separating BOLD and non-BOLD signals while managing thermal noise. This method enhances the accuracy and reliability of fMRI studies, enabling clearer identification of brain networks and reducing the impact of artifacts.

2.4.1 Practical Approaches and Techniques for Denoising fMRI Data

Despite the substantial benefits of ME-fMRI over standard fMRI, it is still not widely adopted. For instance, the spiral and echo planar (SPEP) sequence by Wong et al., available for several years on the GE platform, could flexibly implement ME-fMRI as well as other techniques like echo relaxation imaging. The main practical challenge has been that gradient echo image readout takes too long without in-plane acceleration, causing most signals to dephase by the third TE. Acquiring images with in-plane acceleration is crucial for making ME-fMRI more practical. This method speeds up image readout so that three to five TEs of whole-brain signals can be acquired within a standard TR of 2–3 seconds. Combined with recent developments in multi-band imaging, significantly shorter TRs are achievable. The first widespread use of multi-echo acquisition and analysis was based on the Siemens platform, originating at the F.C. Donders Centre for Cognitive Neuroimaging (Nijmegen, Netherlands) Institute, and affiliated institutions. Despite many successful uses, the spread of the multi-echo approach has been hindered by challenges in managing the multi-TE time series. To address these practical issues, the analysis tool meica.py was developed and distributed to streamline multi-echo analysis, handling all stages of basic and ICA-based ME analysis.

The design intent of meica.py is to simplify ME-fMRI processing, allowing “raw” ME-fMRI data to be input and fully processed BOLD time series and component maps to be output. The pipeline is flexible, enabling analysis with or without an anatomical image, and in standard space or not. It is also open-source, based on the GPL-licensed AFNI and Python tools for open science (available at [available at www.bitbucket.org/prantikk/meica](http://www.bitbucket.org/prantikk/meica)).

There are two main steps in this pipeline. Meica.py itself writes a shell script for preprocessing using AFNI tools. This mostly adapts basic fMRI preprocessing but applies it with TE properties in mind and is designed to keep multi-TE time series aligned. For example, early TE data is used for rigid body motion correction based on having the highest signal intensity across tissues. Based on a sample of ME images from a short series of TRs, optimally combined signals are used to create a mask image by a variant of the BET method. Local Pearson correlation of T2* with the anatomical drives functional-anatomical coregistration [22].

The parameters of motion correction and alignment are combined in one matrix and applied to all TE time series. Band-pass filtering and spatial smoothing are not recommended but are supported. The script then calls another code, tedana.py, which implements several ME analyses such as T2* model fitting and ICA, based on the equations in this manuscript. These functions are built with routines from the Numpy and Scipy Python toolkits. These implementations are efficient by passing computationally intense steps to optimized low-level and parallelized linear algebra codes built into Python toolkits. Tedana.py first does ME-PCA to isolate signals for ICA, by default on optimally combined data. It then finds ICA components using FastICA, implemented with Numpy and Scipy routines. Each component is then processed to compute κ and ϱ , and other accessory component metrics. These additional metrics aid in capturing specific artifacts such as those from in-plane acceleration and draining veins. Finally, components are classified into BOLD and non-BOLD groups and constituted into time series for various processing approaches.

ME-ICA writes three different time series datasets that vary by how strictly BOLD versus non-BOLD signals are retained, with a rationale based on end use (Fig. 6). First are the T2*-weighted “optimally combined” time series, which can be a drop-in replacement for standard fMRI data while benefitting from signal-to-noise ratio boosts of the T2* weighted combination. This data represents all BOLD and non-BOLD signals, and so benefits from some denoising such as motion regression to be useful in most cases.

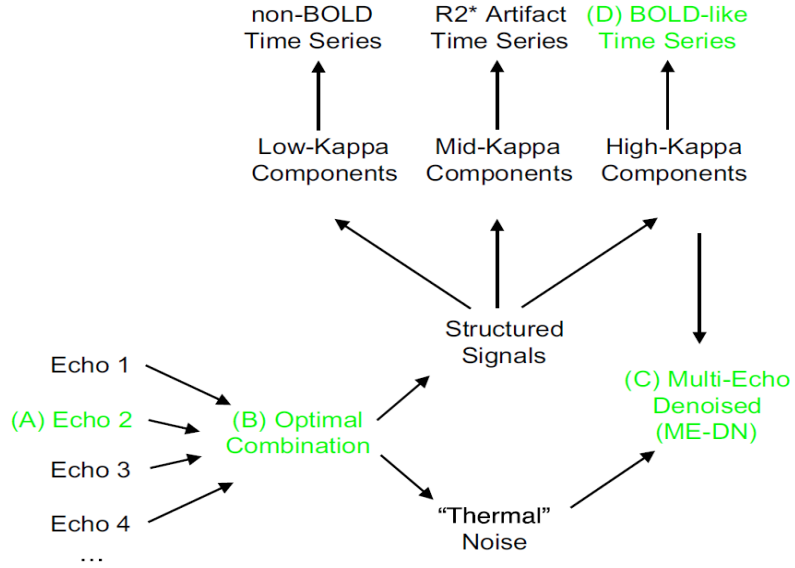


Figure 2.6: Pipeline of component and time series outputs from ME-ICA. Key time series from multi-echo fMRI acquisition and ME-ICA analysis: (A) Time series of "middle" echo, can be used for standard fMRI analysis. (B) Time series after combining echoes, can be used for standard analysis. These time series have enhanced functional contrast and have compensated for dropout artifact. (C) Time series with non-BOLD artifact removed, but retaining Gaussian-like noise. (D) Time series from only BOLD components, suitable for studies of BOLD dynamics [22].

The second time series has non-BOLD and mid- κ ICs removed but retains i) thermal noise, ii) low variance ICs, and iii) ignored ICs. This data, called ME-DN, removes a large portion of nuisance variance by removing a small number of components, far fewer than the number of time points. Good denoising is achieved with a relatively small loss in degrees of freedom. The ME-DN time series are the most efficiently denoised from ME-ICA and are well-suited to voxel-wise general linear modeling (GLM) at the subject level. This is because ME-DN data optimize the balance of low noise and high degrees of freedom, which is crucial for finding significant effects on the basis of T-statistics. However, the number of degrees of freedom does vary across ME-DN datasets, so efforts should be made to account for this variability in subject-level and group-level analyses to avoid inflated test statistics and false-positive findings. In general, the ME-DN data are a safe option for good denoising with many retained degrees of freedom and are the main choice for subject-level model fitting if the software does not support setting degrees of freedom manually (Fig. 7).

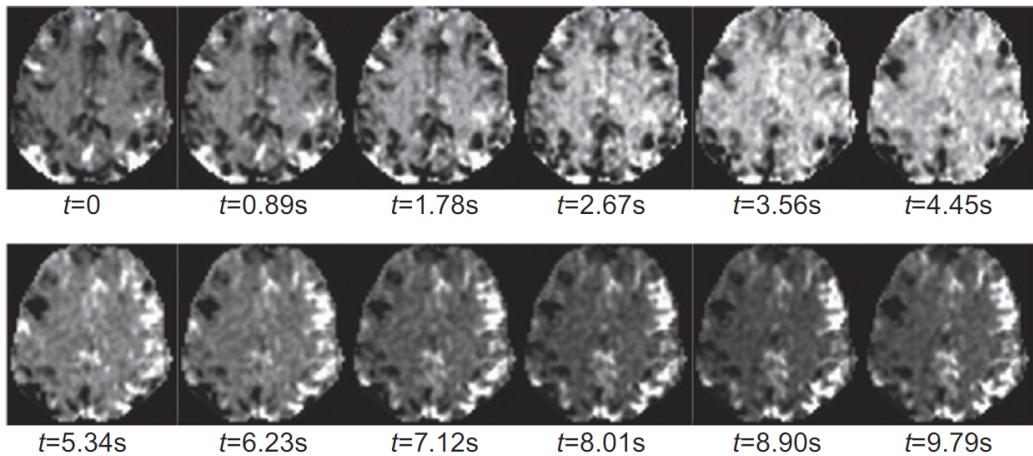


Figure 2.7: Cortical dynamics captured in high- κ time series. Using multi-echo multi-band fMRI sequence with in-plane acceleration factor (GRAPPA) 3, and multi-band factor 3, leading to 2.5 mm isotropic resolution sampled at TR=0.87 s. In evolution over about 10 s, the transition between two states of spontaneous activity is seen.

The third option is BOLD time series recomposed only from BOLD components. These time series, called the high- κ time series, have degrees of freedom equal to the number of BOLD components. High- κ data minimizes the contribution of Gaussian noise, which is a special property. If these data are played as a video, they can show dynamic cortical waves of activity. These data are also suitable for univariate task-based GLM analyses. However, T-statistics are not valid at the subject level if degrees of freedom are not carefully counted, which is not possible in most software. Nevertheless, GLM fit coefficients (β) computed from this data can be passed to group analysis such as using T-test or ANOVA without special considerations (Fig. 8).

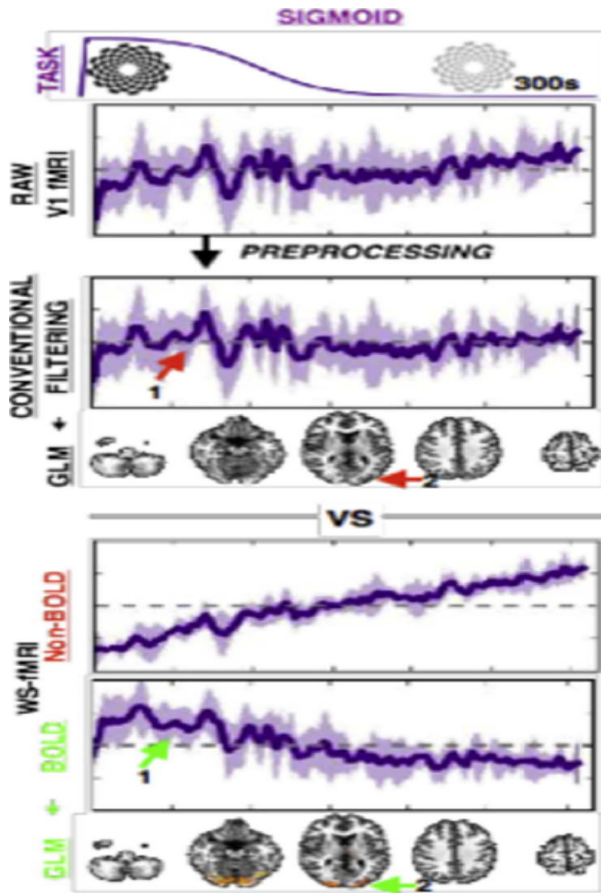


Figure 2.8: Detection of sigmoidal BOLD effect after separating BOLD from non-BOLD signals. Raw fMRI from primary visual cortex during slow visual contrast change does not show slow BOLD change. Conventional time course filtering does not expose a slow varying effect. After ME-ICA, BOLD signal shows sigmoidal effect that localizes to visual cortex. Non-BOLD signal shows linear drift consistent with usual fMRI artifact [16].

Other types of task activity that can be analyzed with ME-ICA include paradigms with very long blocks or other types of low-frequency patterns, with epochs on the order of minutes. This is not possible with single-echo fMRI due to the requirement of a high-pass filter to remove artifactual drift, which is non-specific and removes BOLD-related low-frequency fluctuations as well. The removal of drifts in multi-echo fMRI can be done by removing non-BOLD signals, making it possible to detect low-frequency activity related to BOLD contrast. More complex BOLD responses, such as sigmoidal activations, can also be detected [16].

evoked many such types of activity using visual stimuli with varying visual contrast. These activations were isolated and mapped based on ME-DN time series from ME-ICA. For several types of temporally complex activation models with very-low-frequency components, including sigmoids, activations localized well to the visual cortex, as expected. The possibility of mapping ultra-low frequency fluctuations suggests an opportunity for future studies on the effects of drugs or learning to utilize the enhanced sensitivity to corresponding low-frequency signal changes.

2.5 Graph Theory in Neuroimaging

Graph theory is a branch of mathematics that studies the properties and relationships between nodes (or vertices) and edges (or links) that connect them. This theoretical framework is particularly powerful for analyzing complex systems, including the brain's structural and functional networks. In neuroimaging, graph theory provides a quantitative approach to understanding the brain's connectivity patterns and their implications for cognitive processes and neurological diseases.

2.5.1 Fundamentals of Graph Theory

Graph theory allows researchers to model the brain as a network where nodes represent brain regions and edges represent the connections between them. This representation enables the analysis of various properties of brain networks, such as connectivity strength, efficiency, and resilience. Key concepts in graph theory include:

- Nodes (Vertices): Represent distinct brain regions or functional units.
- Edges (Links): Represent the connections or interactions between nodes, which can be structural (anatomical) or functional (based on correlated activity).
- Degree: The number of connections a node has. Nodes with high degrees are considered hubs and play crucial roles in network connectivity.
- Path Length: The shortest path between two nodes. Shorter path lengths indicate more efficient communication.
- Clustering Coefficient: Measures the degree to which nodes tend to cluster together. High clustering is often associated with specialized processing regions.
- Modularity: The extent to which a network can be divided into modules or communities with dense intra-connections and sparse inter-connections [10].

2.5.2 Using Graph Theory to Quantify Resting-State Connectivity

Graph theory has been instrumental in quantifying resting-state connectivity in the brain. Resting-state fMRI (rs-fMRI) measures spontaneous brain activity, providing insights into the brain's functional organization during rest. By applying graph theory to rs-fMRI data, researchers have identified key network properties such as hubs, modularity, and efficiency that characterize the brain's intrinsic connectivity. Graph theoretical measures like degree centrality, clustering coefficient, and path length have been used to quantify how brain regions (nodes) are interconnected (edges) and how these connections form complex networks. For instance, degree centrality helps identify crucial brain regions that act as hubs, facilitating communication across the network. Clustering coefficient measures how nodes form tightly knit clusters, indicative of specialized processing regions, while path length assesses the efficiency of information transfer across the brain [10, 32].

Studies have demonstrated that resting-state networks (RSNs) exhibit small-world properties, which balance high local clustering and short path lengths, enhancing both specialized and integrative processing [10, 32]. Graph theoretical analysis of rs-fMRI data has also revealed distinct connectivity patterns associated with various cognitive functions and neurological conditions [38]. For instance, alterations in network properties have been linked to disorders like schizophrenia, Alzheimer's disease, and autism spectrum disorders, providing potential biomarkers for diagnosis and treatment [36, 8, 42]. These analyses have shown that in Alzheimer's disease, there is a disruption in the efficiency of brain networks, whereas in schizophrenia, there is often a reduction in the global connectivity of the brain network. Overall, the integration of graph theory with rs-fMRI offers a robust framework for understanding the complex architecture and functional dynamics of the brain.

Chapter 3

Methodology

3.1 Dataset

Data were obtained from 20 subjects, collected from consenting neurotypical subjects with standard inclusion/exclusion criteria (English speaking, right-handed, no history of neurological or psychiatric illness) and the protocol was approved by the Cambridge IRB (LREC 11/EE/0198). BOLD data were collected with subjects' eyes open at rest, looking at a white screen. The data was sourced from the OpenNeuro dataset, which includes multi-echo BOLD fMRI scans. The dataset consists of 4 echoes of a single 9.84-minute multi-echo BOLD run. [27]

Subject Information

- Body Part Examined: Head
- Magnetic Field Strength: 3 Tesla
- Manufacturer: Siemens
- Model Name: Trio
- Receive Coil Name: 32-Channel Head Coil
- Task Name: Rest

fMRI Acquisition Parameters

- Echo Time (TE): 12, 28, 44, and 60 ms
- Number of Echoes: 4
- Repetition Time (TR): 2.47 seconds
- Flip Angle: 78 degrees
- Pixel Spacing: 3.75 mm (in-plane), 4.4 mm (slice thickness)

- Pixel Bandwidth: 1698 Hz/Px
- Parallel Reduction Factor In-Plane: 3
- Slice Thickness: 4.4 mm
- Spacing Between Slices: 4.84 mm
- Slice Timing: [1.235, 0.000, 1.317, 0.082, 1.399, 0.165, 1.482, 0.247, 1.564, 0.329, 1.647, 0.412, 1.729, 0.494, 1.811, 0.576, 1.894, 0.659, 1.976, 0.741, 2.058, 0.823, 2.141, 0.906, 2.223, 0.988, 2.305, 1.070, 2.388, 1.153 seconds]

3.2 Multi-Echo denoising

Effective denoising is crucial for the success of this project, as it is imperative to remove all non-BOLD components from the fMRI data before constructing the final state machine of the brain. This process ensures that the data used for analysis accurately reflects the neural activity of interest, free from artifacts and noise that could otherwise compromise the integrity of the results.

In this research, a new and updated version of Multi-Echo Independent Component Analysis (MEICA) was used for denoising functional MRI (fMRI) data. This process is facilitated by the tedana package, developed by the MEICA group, which requires Python 3.6+ [29]. The script, written in tcsh, utilizes afni_proc.py to preprocess and denoise the fMRI data.

3.2.1 Explanation of Denoising Methods

1. Despiking: The despikes block removes transient high-intensity artifacts (spikes) from the fMRI time series, which can result from sudden head movements or scanner noise.
2. Time Shifting (Slice Timing Correction): The tshift block corrects differences in slice acquisition times by temporally aligning the slices within each volume. This is achieved using sinc interpolation with the -wsinc9 option.
3. Alignment (Motion Correction): The align block adjusts the fMRI volumes to correct for head motion across the time series. The alignment options -cost lpc+ZZ -giant_move -check_flip ensure robust correction, accommodating large movements and checking for left-right flips.
4. Normalization to Template (Talairach Transformation): The tlrc block aligns the functional data to the MNI152 template (MNI152_2009_template_SSW.nii.gz), facilitating comparison across subjects and studies.

5. Volume Registration: The volreg block performs volume registration, aligning each time point to the volume with the minimum outlier fraction (MIN_OUTLIER). This ensures that the data is consistently positioned in space.
6. Masking: The mask block creates a brain mask to isolate brain tissue from non-brain areas, improving the accuracy of subsequent analyses.
7. Combining Echoes: The combine block integrates multi-echo data using the optimal combination (OC) method. This enhances the signal-to-noise ratio (SNR) by combining the echoes weighted by their respective SNRs.
8. Spatial Smoothing: The blur block applies a small Gaussian blur (FWHM = 3mm) to the data to improve SNR while preserving spatial resolution.
9. Intensity Normalization: The scale block normalizes the voxel time series to a common scale, typically converting them to percent signal change.
10. Regression: The regress block includes several important steps:
 - Motion Regression: Removes motion-related variance by including motion parameters as regressors.
 - Censoring: Excludes time points with excessive motion ($\$cen_motion = 0.2$) or outliers ($\$cen_outliers = 0.05$).
 - Trend Removal: Uses polynomial detrending to remove low-frequency drifts and high-frequency noise.
 - Blur Estimation: Estimates the smoothness of the residuals and the data, informing the statistical analysis.
11. Radial Correlation: The radial_correlate_blocks option computes the correlation between each voxel's time series and the mean time series within a radial sphere, enhancing the detection of functional connectivity patterns.

By employing these comprehensive denoising techniques, the MEICA approach ensures that the resulting fMRI data is of high quality, with reduced noise and artifacts, allowing for more accurate and reliable analysis of brain function [29].

3.3 Identifying Resting-State Networks (RSNs) Using Independent Component Analysis(ICA)

After converting the cleaned fMRI data to NIfTI format, the next step involved running MELODIC (Multivariate Exploratory Linear Optimized Decomposition into Independent Components) in FSL (FMRIB Software Library). MELODIC is a tool for performing Independent Component Analysis (ICA) on fMRI data, which is used to identify resting-state networks (RSNs) within the brain [4].

MELODIC decomposes the fMRI data into spatially independent components (ICs), which correspond to different functional networks and artifacts. These independent components represent distinct patterns of brain activity that are statistically independent from each other. Some of these components correspond to RSNs, such as the Default Mode Network, Visual Network, and Sensorimotor Network. This process allows researchers to separate meaningful brain activity from noise and other confounding signals. The output of MELODIC includes maps of the identified components and their associated time courses, which are critical for subsequent analyses [3].

The identified RSNs, such as the Default Mode Network, Visual Network, and others, were used in subsequent analyses to study brain connectivity and function. By using MELODIC in FSL, these networks were robustly and efficiently identified and analyzed, providing insights into the brain's intrinsic connectivity [35]. MELODIC produced spatial maps and time courses for each independent component.

In the next step the components were identified corresponding to resting-state networks based on their spatial patterns and temporal characteristics, a rigorous selection process was undertaken due to data quality issues. Out of the initial 20 subjects available, only 6 were deemed suitable for further analysis. For each of these selected subjects, a single appropriate component was chosen for each network. The networks analyzed encompassed the Default Mode Network, Motor Network, Visual Network, Right Executive Network, Left Executive Network, Gray Matter Network 1, and Gray Matter Network 2.

3.3.1 Component Map of resting-state networks

The resting-state networks (RSNs) identified for each subject are illustrated in the figures below. Each network is depicted to demonstrate the spatial patterns and temporal characteristics across the selected subjects.

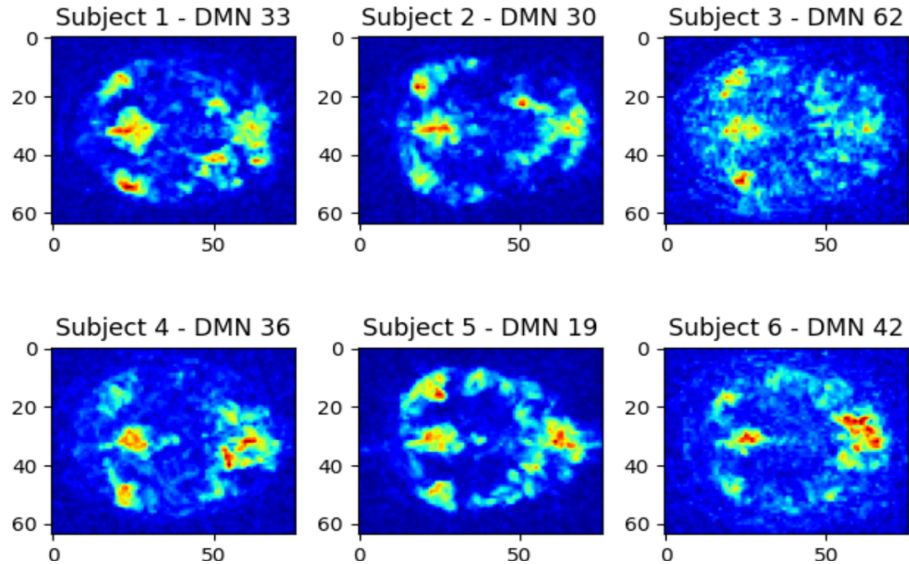


Figure 3.9: Default Mode Network.

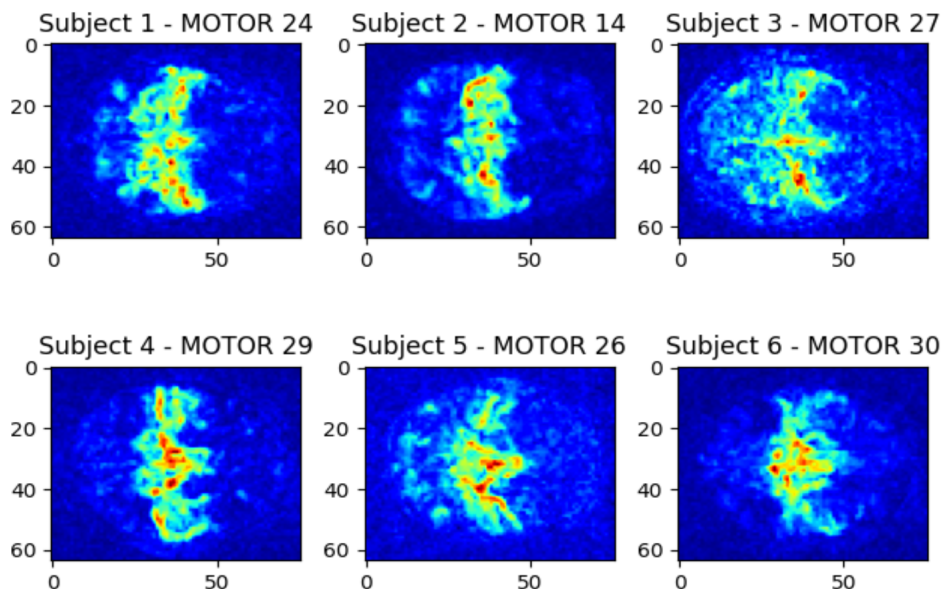


Figure 3.10: Motor Network.

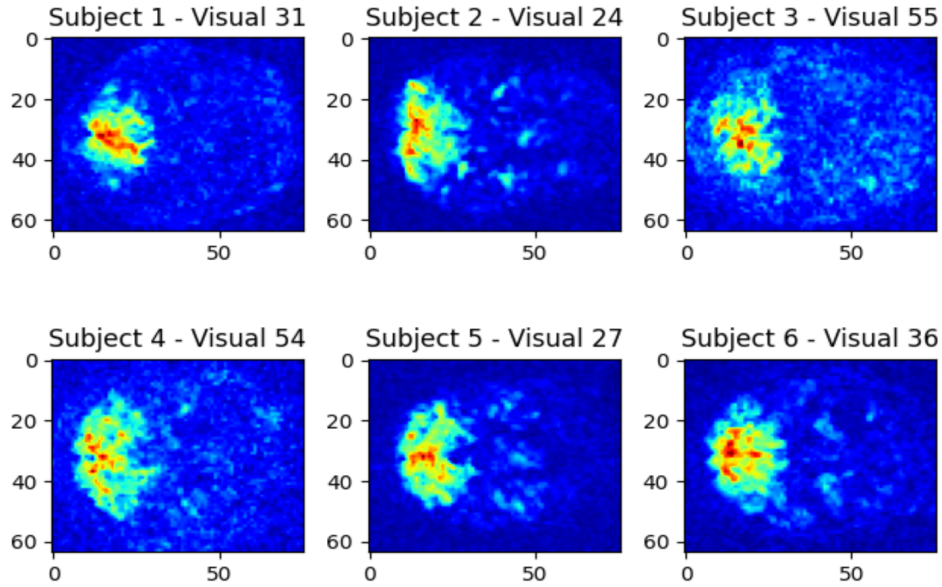


Figure 3.11: Visual Network.

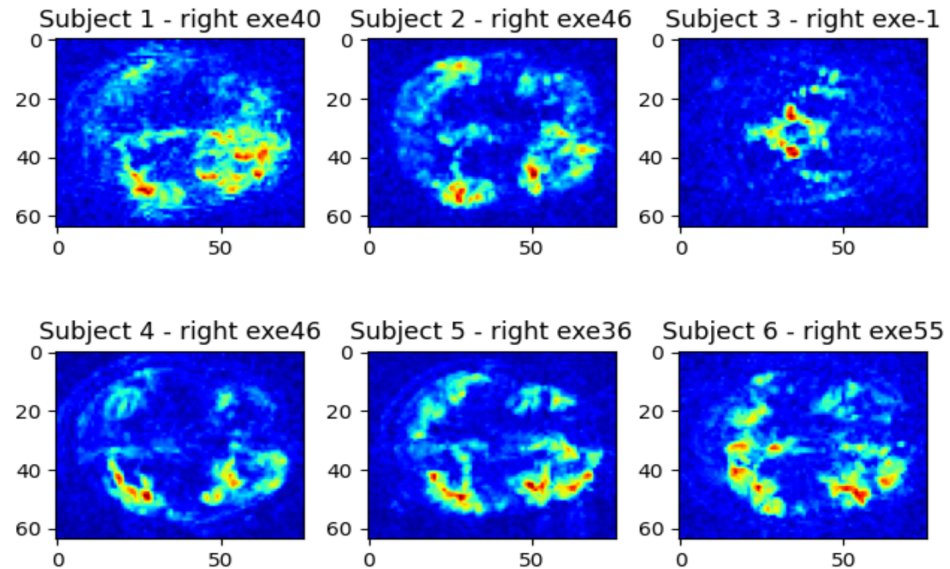


Figure 3.12: Right Executive Network. This network in Subject 3 has some missing values, so it is excluded from Subject 3 in the next analysis.

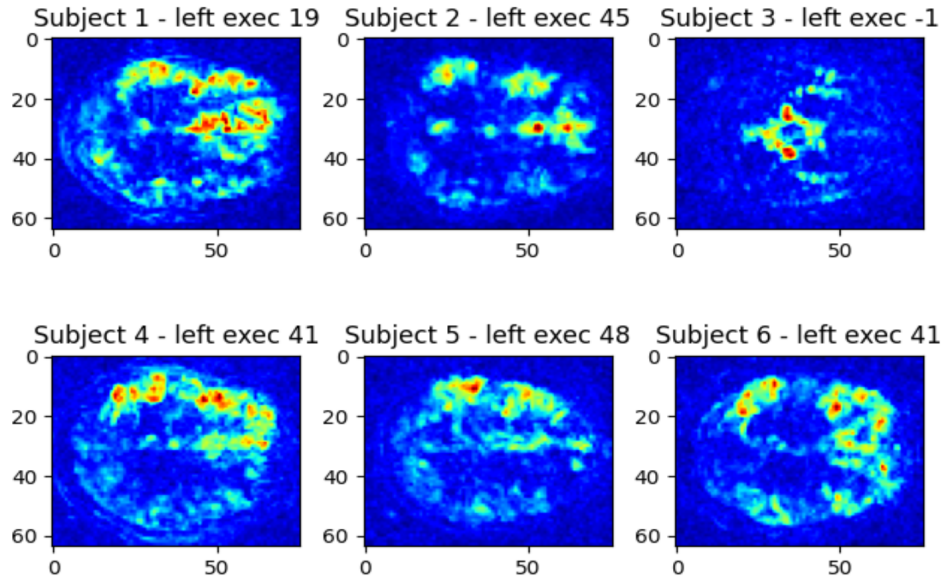


Figure 3.13: Left Executive Network. This network in Subject 3 has some missing values, so it is excluded from Subject 3 in the next analysis.

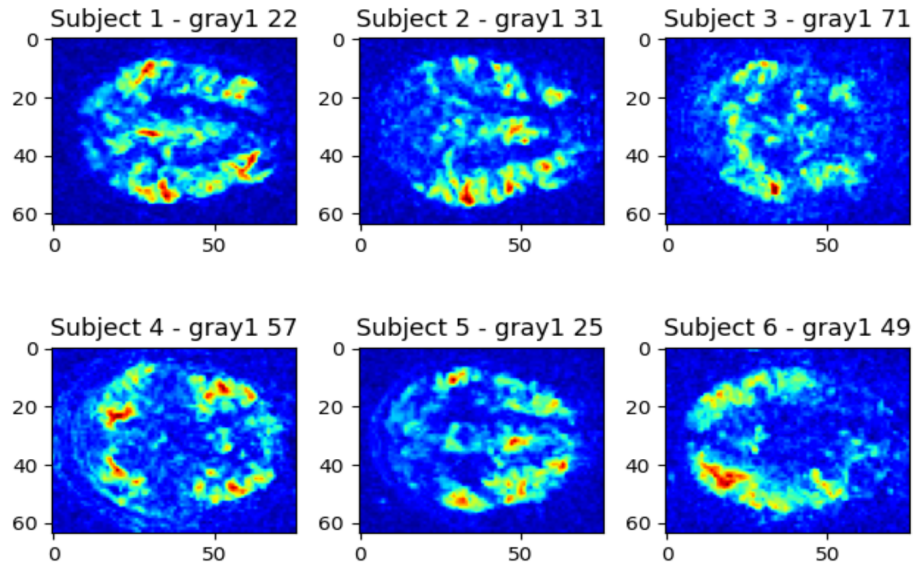


Figure 3.14: Gray Matter Network 1.

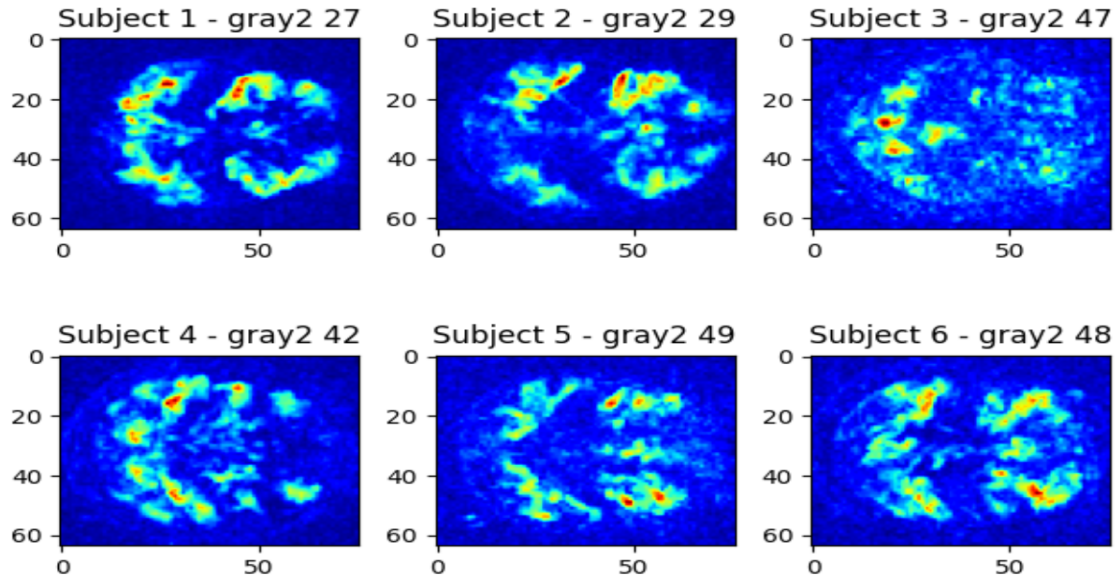


Figure 3.15: Gray Matter Network 2.

3.3.2 Creating Spatial Masks and Isolating Time Series

In the final step of data preprocessing and analysis for the resting-state networks (RSNs), a detailed procedure was undertaken to ensure the accuracy and robustness of the results. Initially, the independent components (ICs) obtained from the MELODIC output were loaded alongside the original fMRI data, which was stored in NIfTI format. The ICs represented spatially independent components derived from the multi-echo fMRI data, essential for identifying the different networks within the brain.

To begin, the indices corresponding to various networks were defined. These indices included the Default Mode Network (DMN), Motor Network, Visual Network, Right Executive Network, Left Executive Network, and two Gray Matter Networks. Each index was associated with a specific component, allowing for targeted analysis of these networks.

Subsequently, a visualization of the independent components was conducted to verify the spatial patterns and ensure that the identified components accurately represented the expected brain networks. This step was crucial for validating the integrity of the data before proceeding with further analysis.

The next critical phase involved creating spatial masks for each component. This was achieved by applying a z-score transformation to the component maps. Z-score thresholding was utilized, with a threshold of $z > 5$ applied to all voxels. This

thresholding process helped isolate the significant regions within each component, effectively creating a mask that highlighted the areas of interest corresponding to each network.

This phase was meticulously executed for each of the six subjects, ensuring comprehensive and precise application across the dataset. The masks for each Network component and each subject are illustrated in the figures below. Also, subject 3 is leaved out from Right Executive Network and Left Executive Network because it was missing such networks.

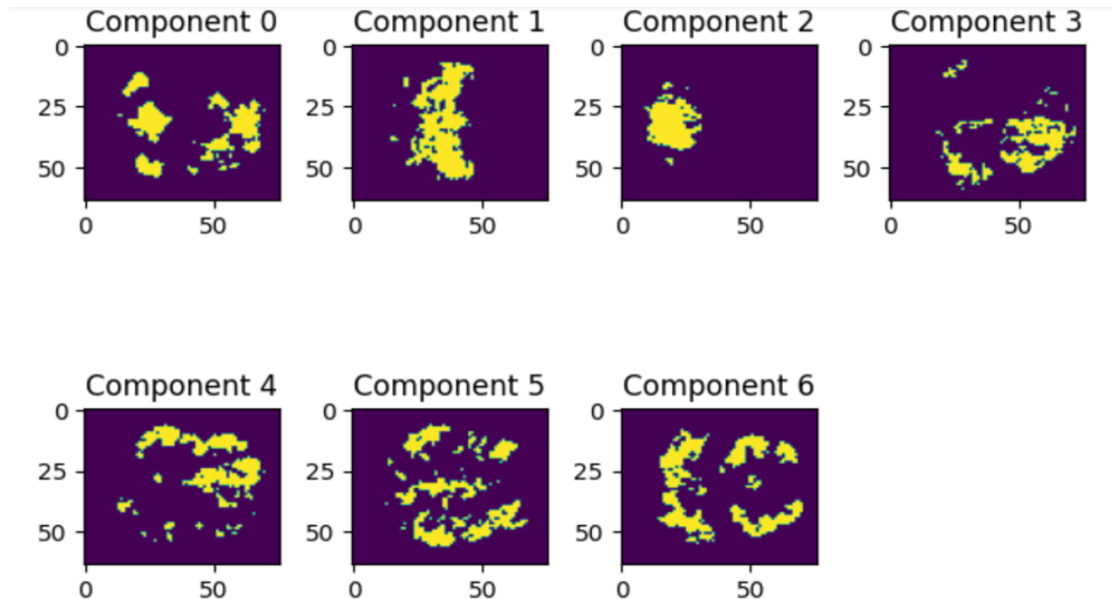


Figure 3.16: Brain Network Component Mask for Subject 1.

In the Masks figures, Component 0 to component 6 refer to Default Mode Network, Motor Network, Visual Network, Right Executive Network, Left Executive Network, Gray Matter Network 1, and Gray Matter Network 2 respectively.

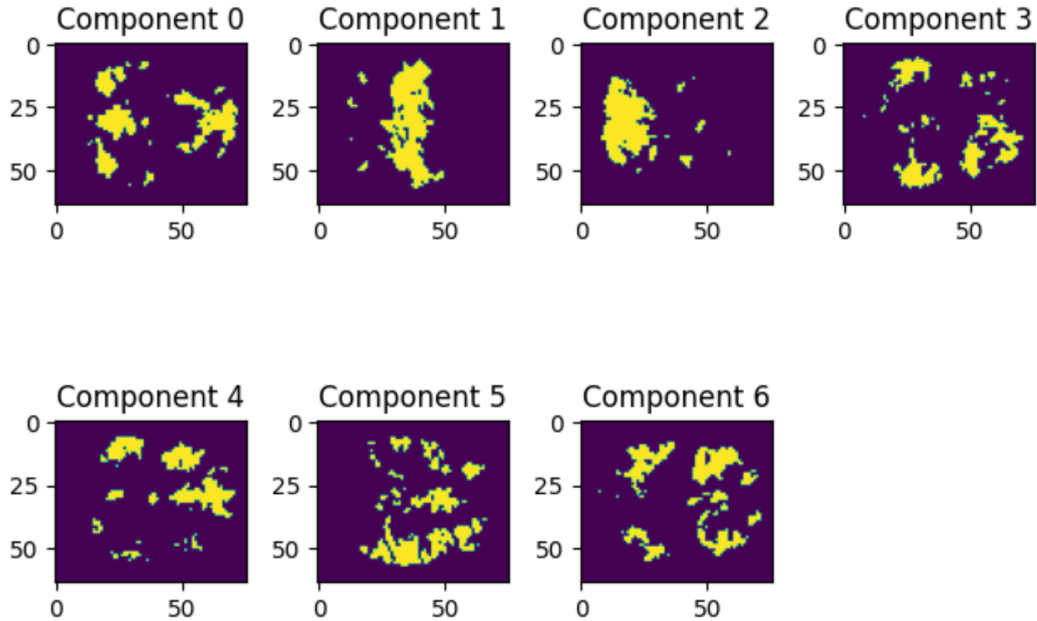


Figure 3.17: Brain Network Component Mask for Subject 2.

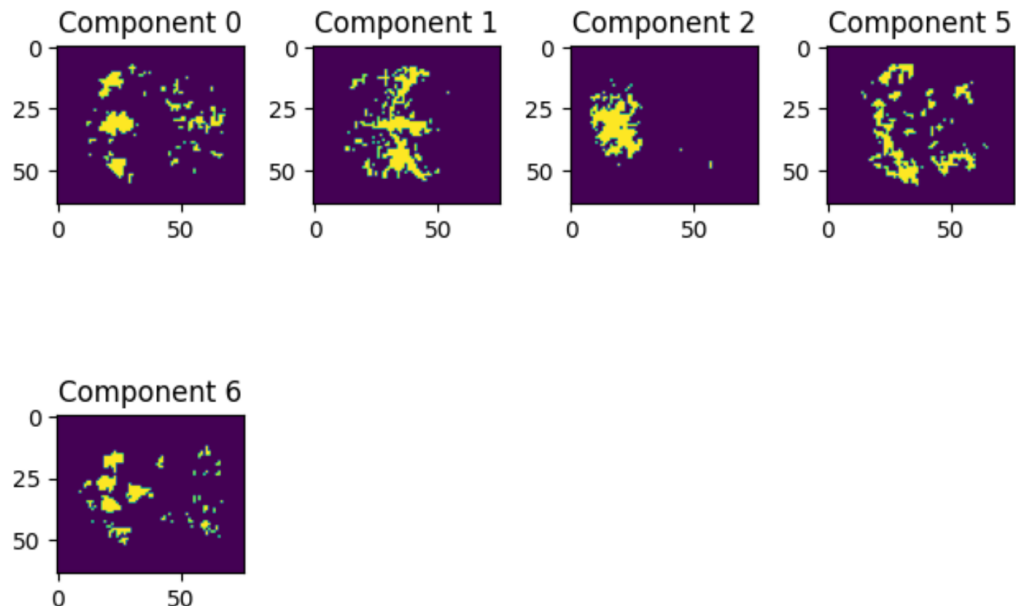


Figure 3.18: Brain Network Component Mask for Subject 3.

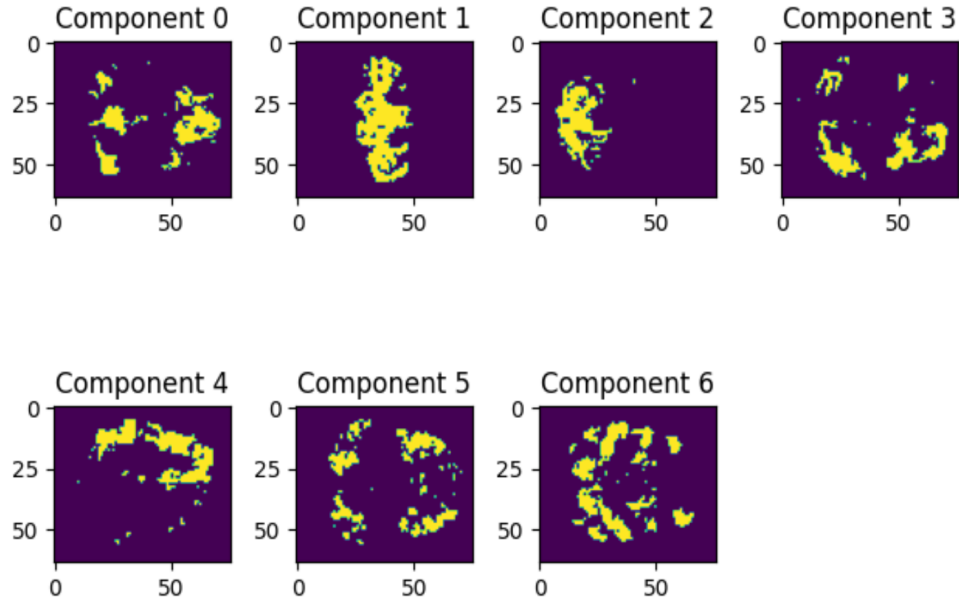


Figure 3.19: Brain Network Component Mask for Subject 4.

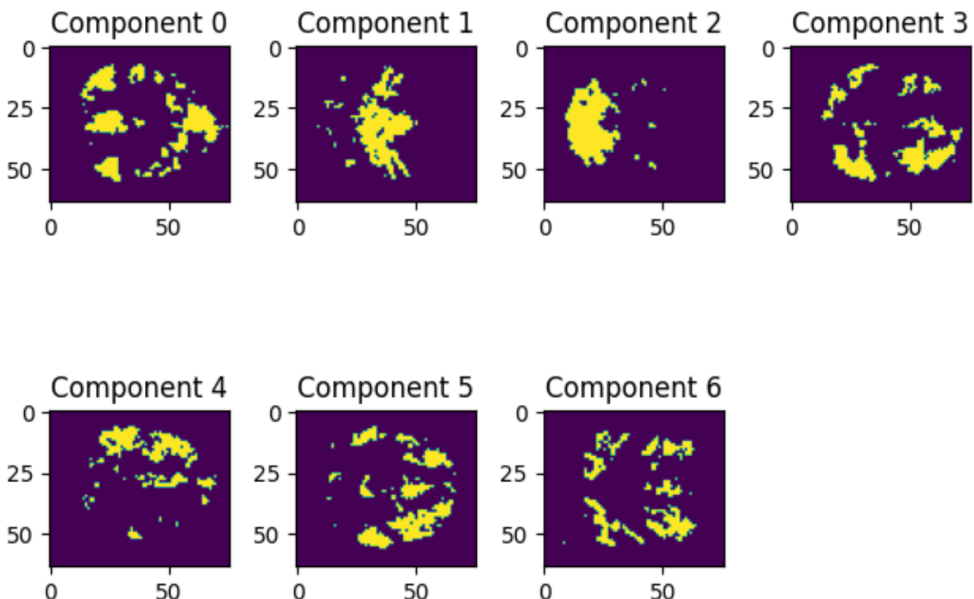


Figure 3.20: Brain Network Component Mask for Subject 5.

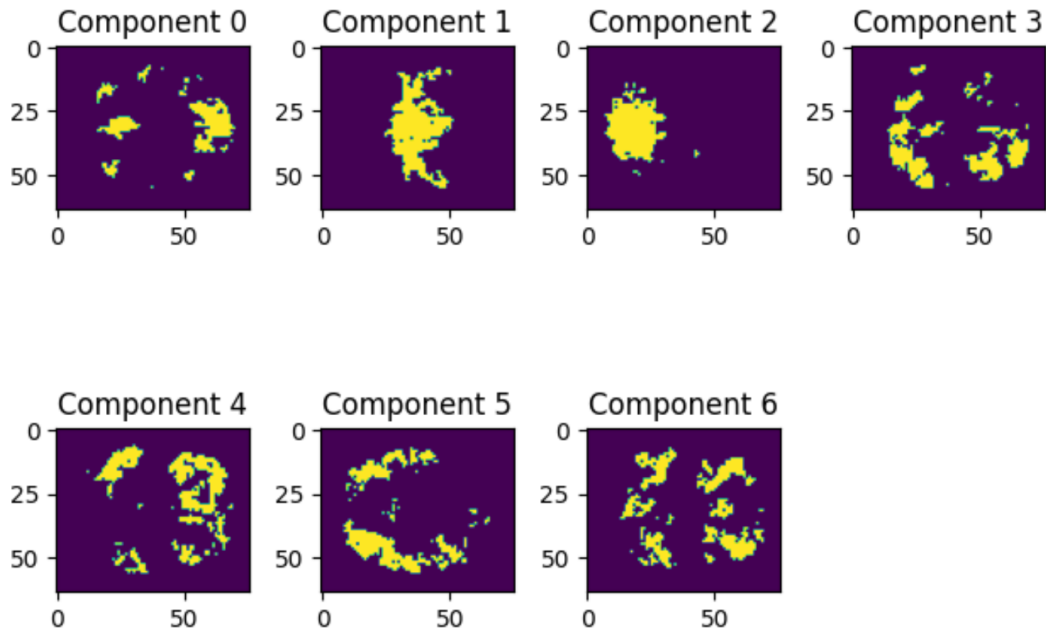


Figure 3.21: Brain Network Component Mask for Subject 6.

Subject 3 is excluded from the Right Executive Network and Left Executive Network analysis due to missing data. Once the spatial masks were established, they were used to isolate the time series from the original fMRI data that were unique to each component mask. By applying these masks to the original data, the time series specific to the regions of interest were extracted. The extracted time series were then averaged across all voxels within the mask to obtain a representative time series for each network component.

To enhance the quality of the time series data, a smoothing process was applied. Gaussian filtering was employed to reduce noise and improve the signal-to-noise ratio, resulting in a clearer and more interpretable time series. This smoothing step was essential for ensuring that the temporal characteristics of the networks were accurately captured.

Finally, the smoothed time series for each network component were plotted and used for further analyses.

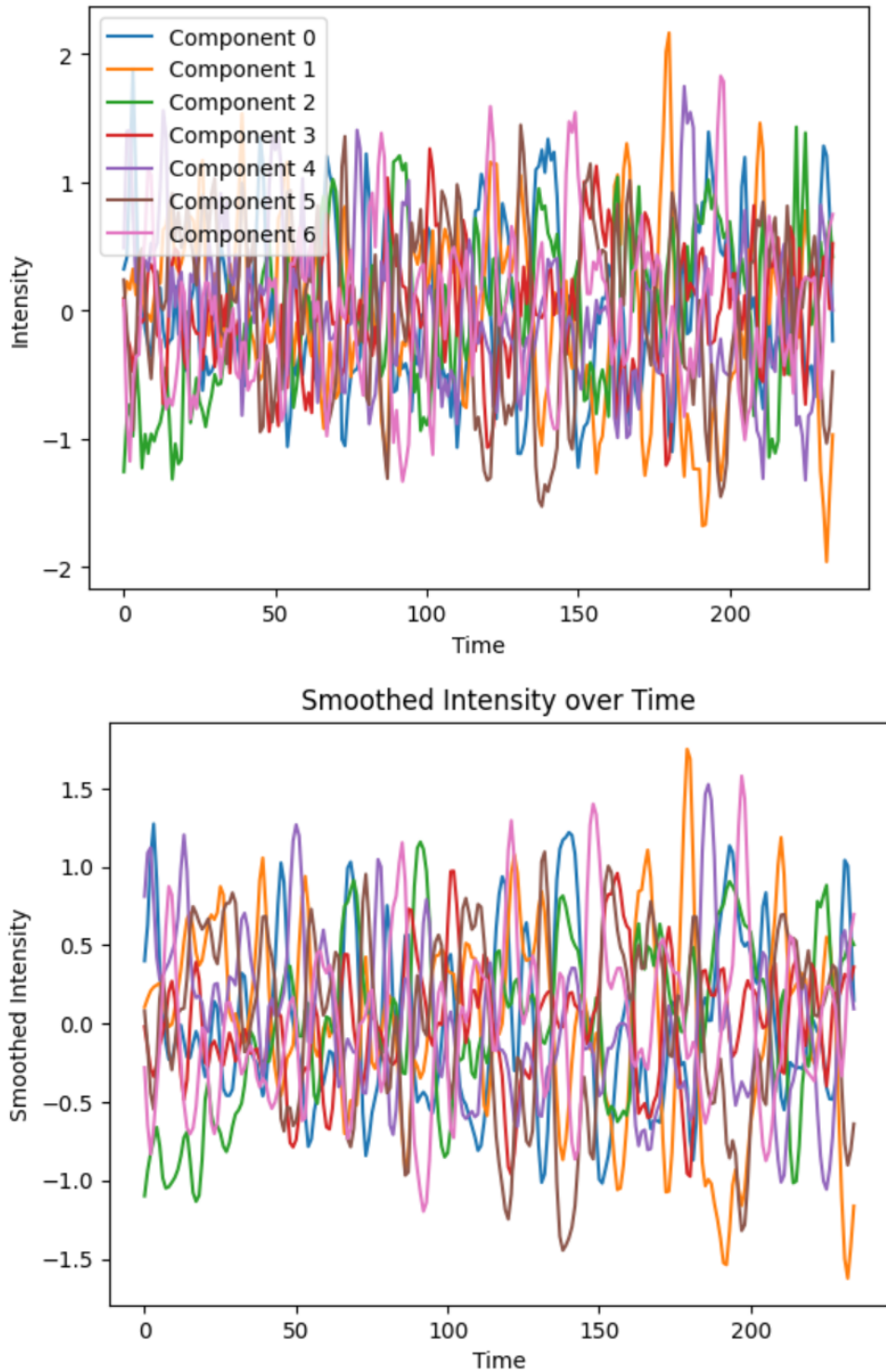


Figure 3.22: Time series for all network components of Subject 1.

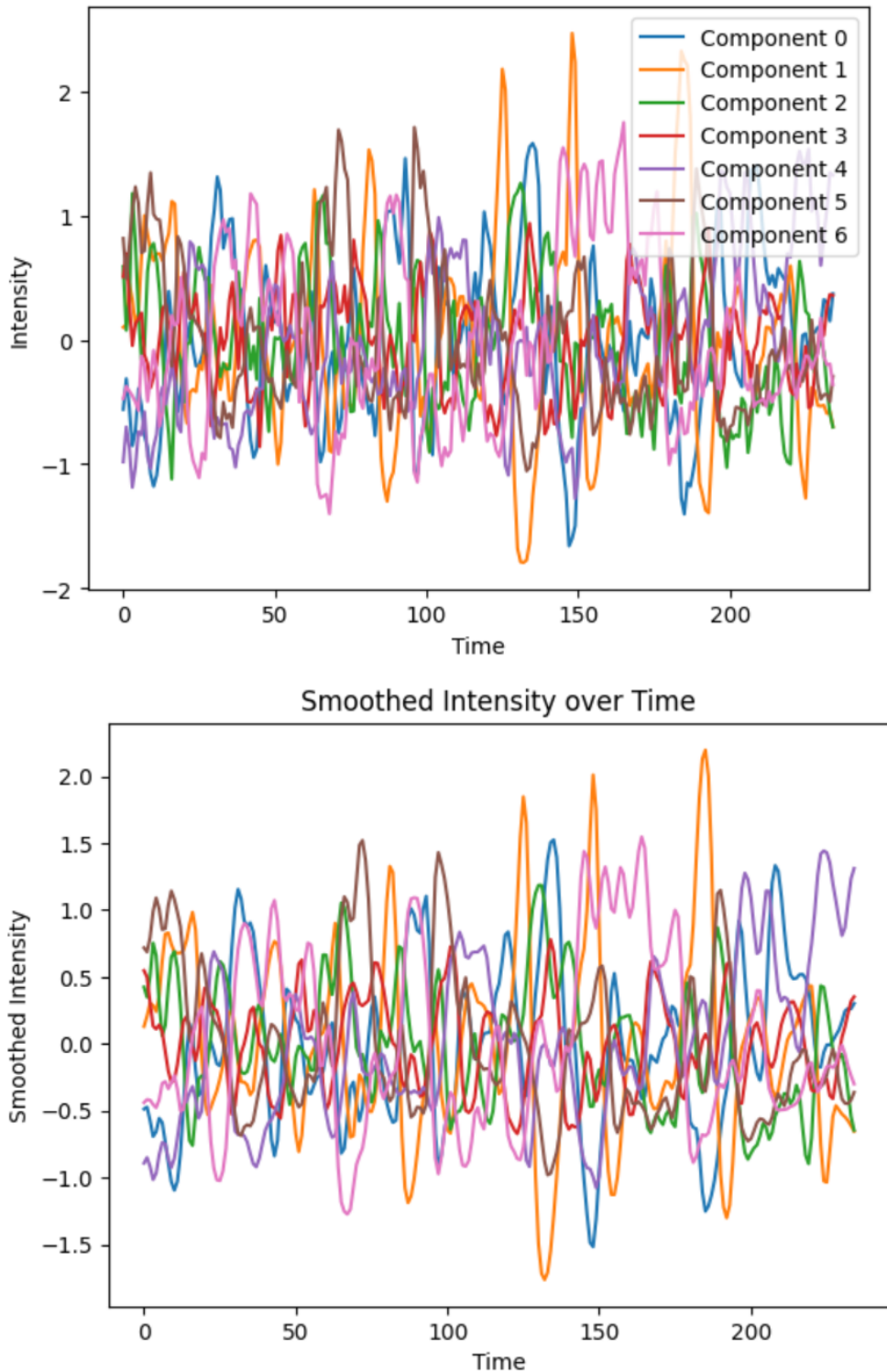


Figure 3.23: Time series for all network components of Subject 2.

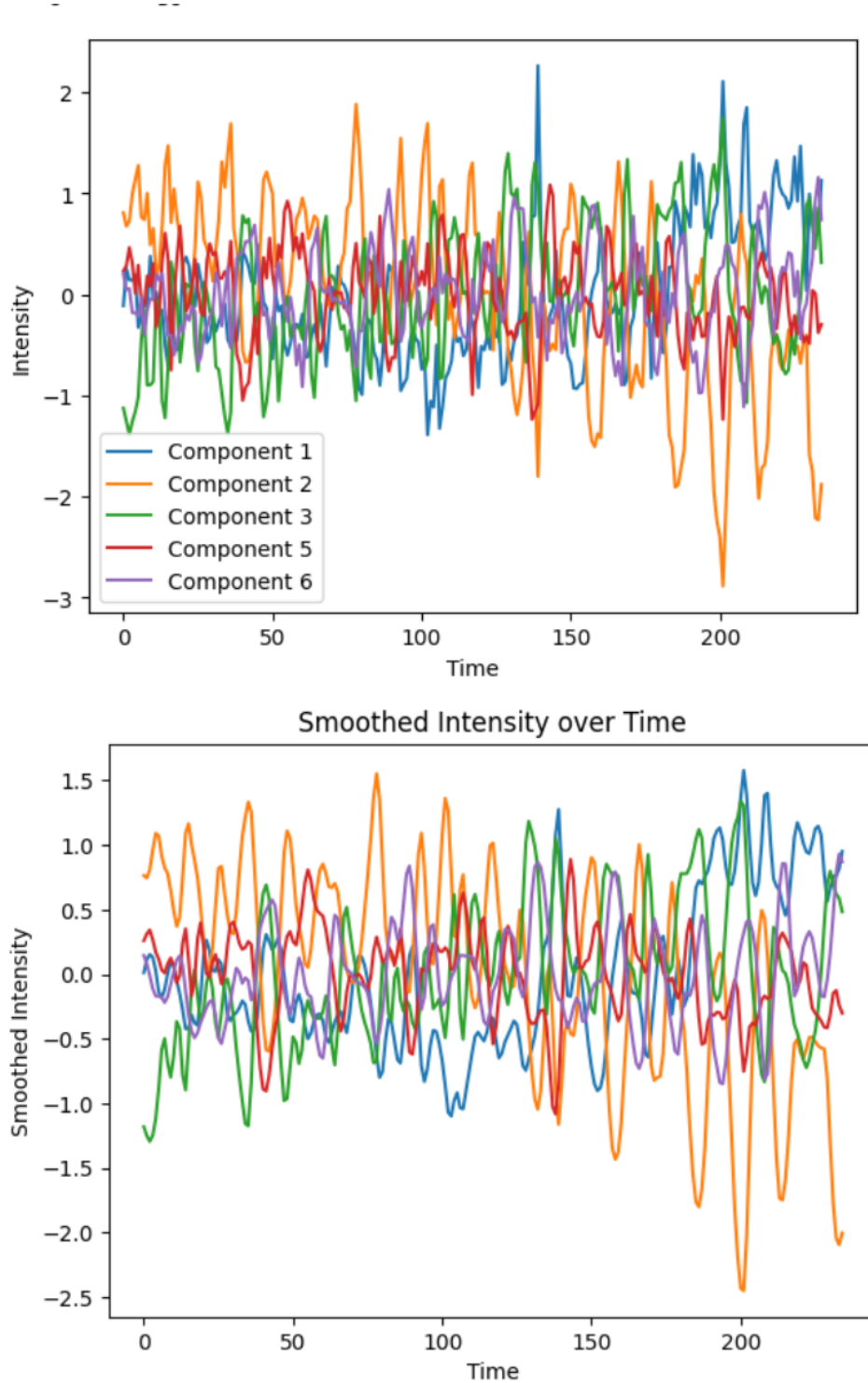


Figure 3.24: Time series for all network components of Subject 3. Subject 3 is excluded from the Right Executive Network and Left Executive Network analysis due to missing data.

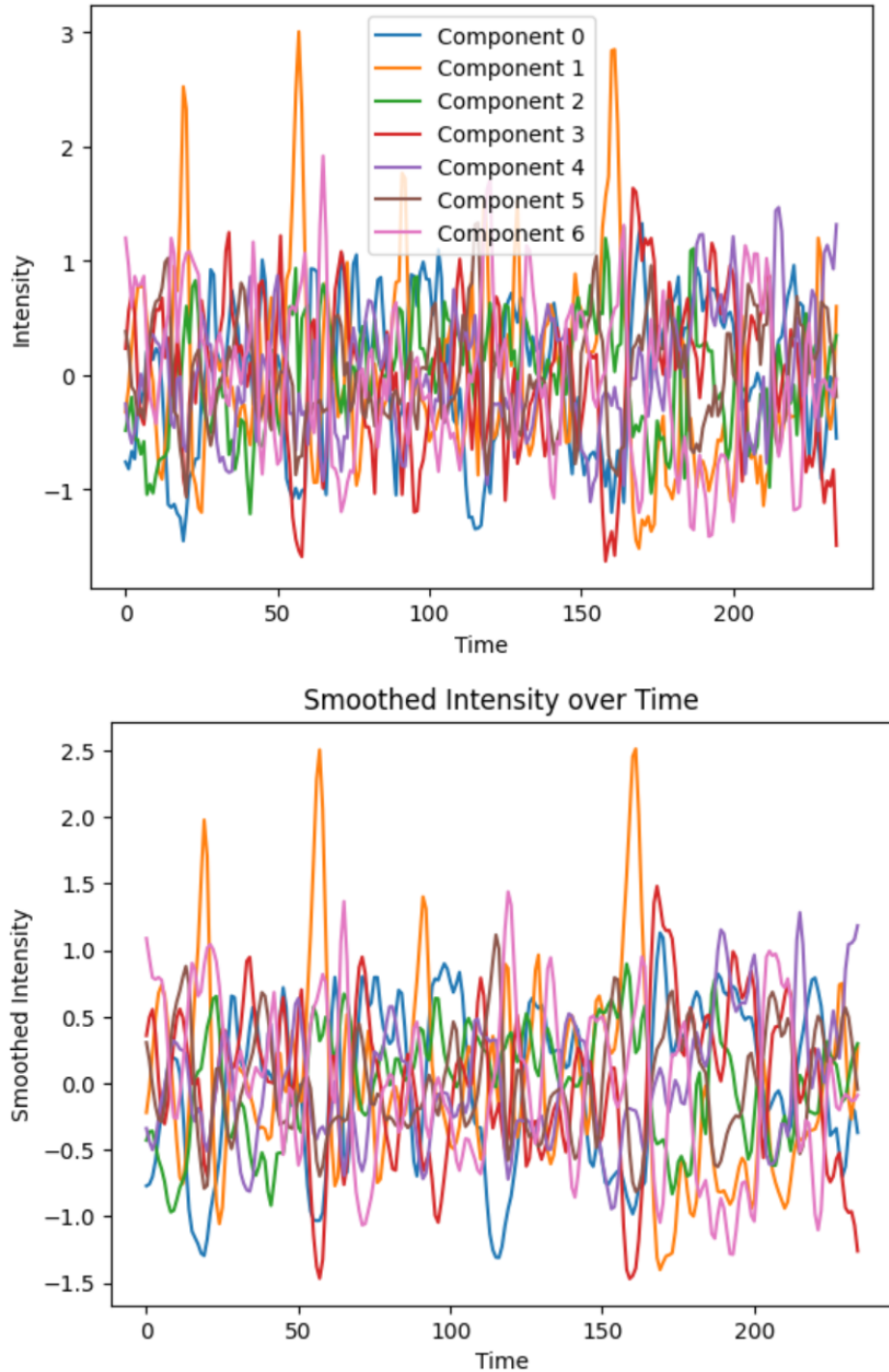


Figure 3.25: Time series for all network components of Subject 4.

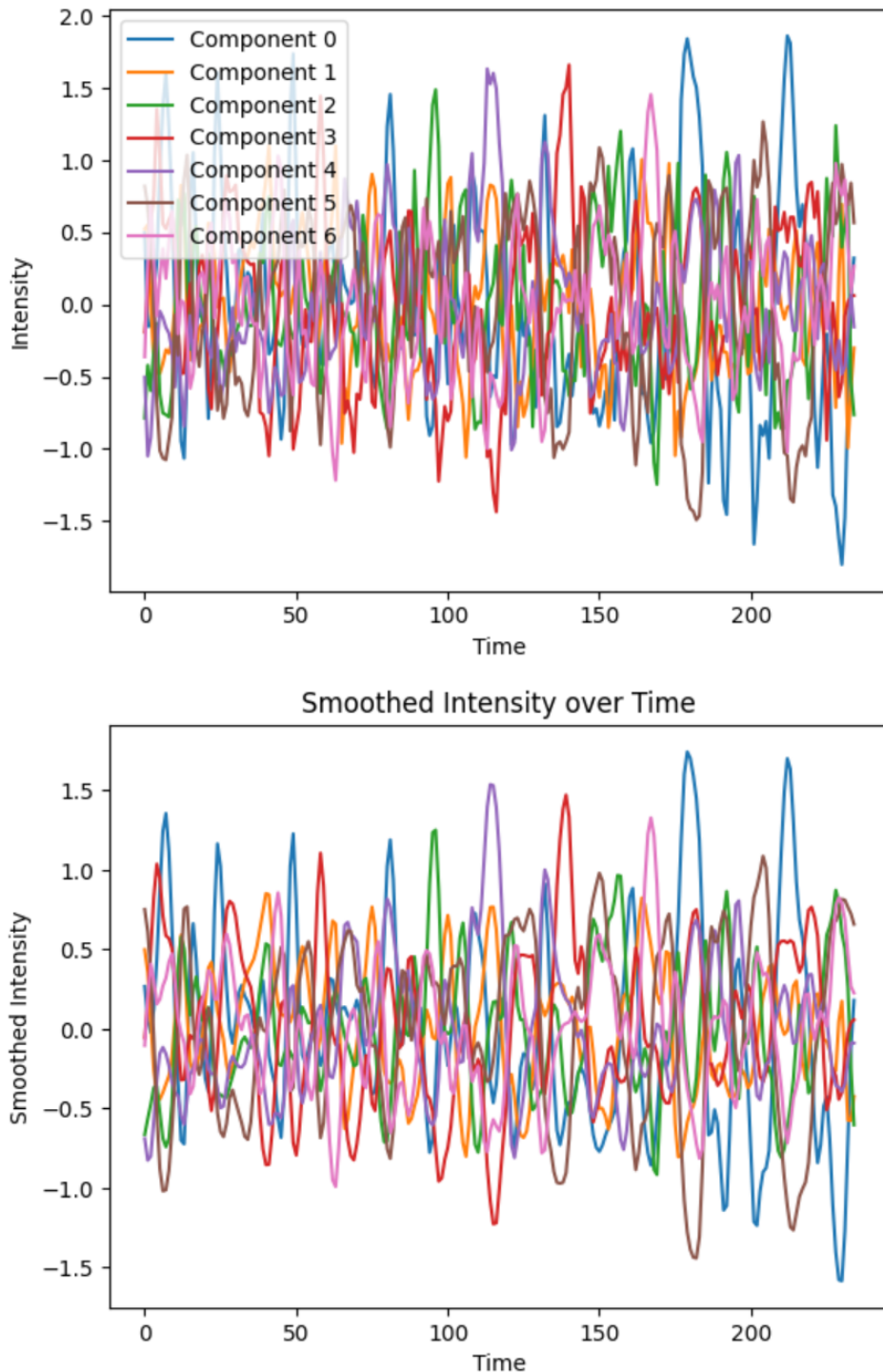


Figure 3.26: Time series for all network components of Subject 5.

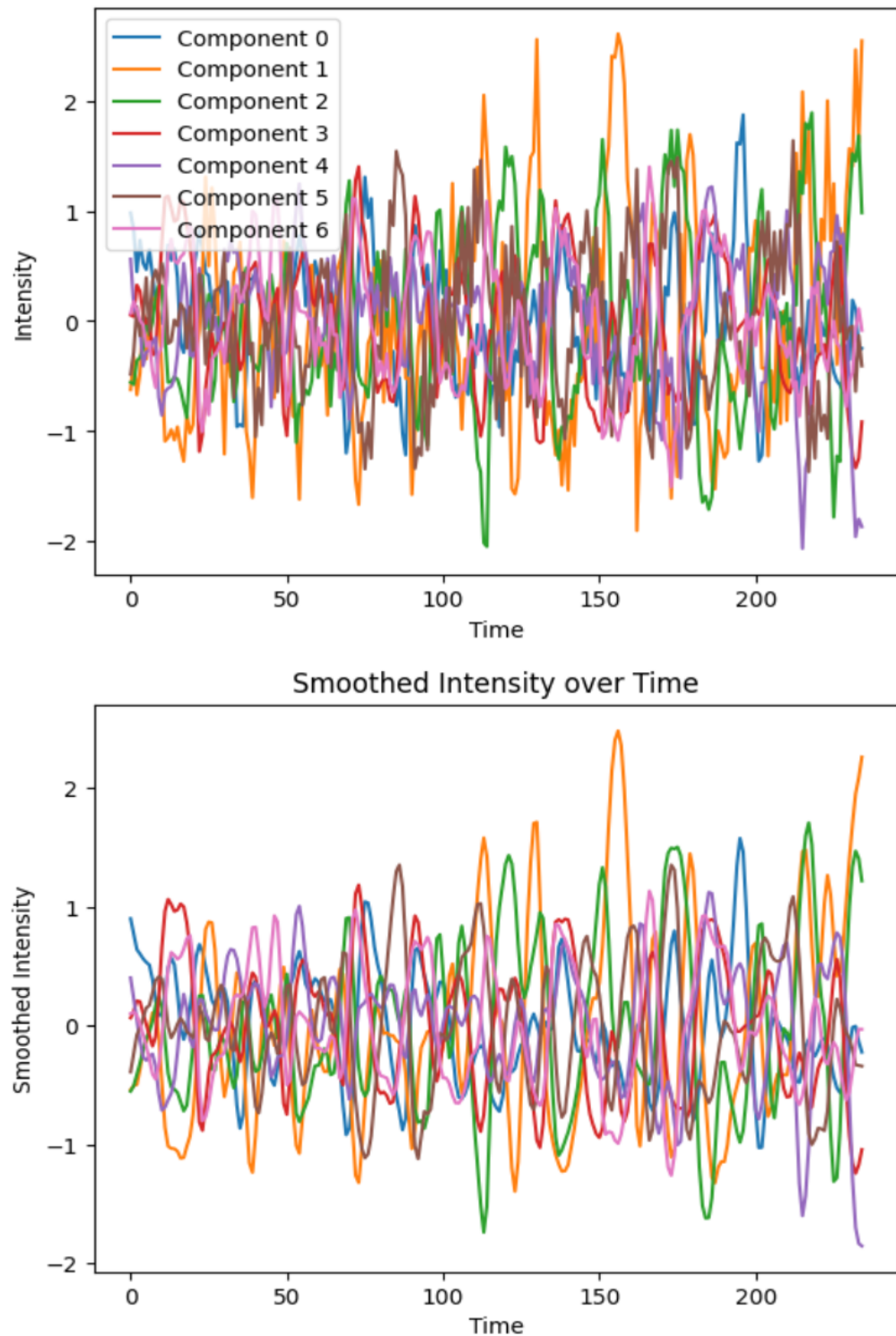


Figure 3.27: Time series for all network components of Subject 6.

In the above figures intensity reflects the level of blood-oxygen-level-dependent (BOLD) signal, which is an indirect measure of neural activity. This comprehensive approach allowed for a detailed examination of the temporal dynamics of the identified resting-state networks, providing valuable insights into the functional connectivity and activity patterns within the brain.

By meticulously following these steps, the final analysis ensured that the resting-state networks were accurately identified and characterized, paving the way for subsequent analyses and interpretations of the data like Creating FSM (Final State Machines) using graph theory.

3.4 Finite state machine construction

In this part, the methodology for determining when the brain transitions between different Independent Component Analysis (ICA) components is elaborated, along with the subsequent construction of a Finite State Machine (FSM) to model these transitions. This analysis provides insights into the dynamic functional connectivity of the brain.

The process began by identifying the point at which the brain switches from one ICA component to another. This was achieved by analyzing the amplitude of the smoothed signal for each component over time. At any given time point, the component with the highest amplitude was considered the 'active' component. A transition was defined to occur when the amplitude of another component surpassed that of the currently active component. For each subject, this transition identification process was meticulously carried out [4].

Once the transitions were identified for each subject, an FSM with seven states was constructed. Each state in the FSM represented one of the ICA components. The transitions between states were quantified by counting the number of times the brain switched from one component to another. The probability of transitioning between different states was calculated by dividing the number of transitions between any two states by the total number of transitions observed [23].

To ensure comprehensive analysis, the transition probabilities were computed for each subject individually. The following steps were undertaken:

1. Maximum Amplitude Component Identification: For each time point, the component with the highest smoothed amplitude was identified, marking the 'active' component at that time.
2. Transition Counting: A dictionary was initialized to count the transitions between different states. For each pair of consecutive time points, if the active component changed, a transition was recorded in the dictionary.

3. Transition Probability Calculation: The total number of transitions was summed, and the transition probabilities were computed by dividing the count of each transition by the total number of transitions.
4. Summation of Probabilities Across Subjects: The transition probabilities were calculated separately for each subject. These probabilities were then summed across all subjects to compute the mean transition probabilities.
5. Calculation of Mean Probabilities: The mean transition probabilities were calculated by dividing the summed probabilities by the total number of subjects, which in this study was six, ensuring that the averaged probabilities accurately represented the transition dynamics across all subjects [35].
6. Normalization of Probabilities: The summed probabilities for each state were normalized to ensure that the sum of probabilities for outgoing transitions from any given state equaled one. This was achieved by dividing each transition probability by the total sum of outgoing probabilities for the respective state [20].

3.4.1 Mathematical Equations to Calculate Transitions and Their Probabilities

To calculate transitions and their probabilities from fMRI data, the following steps are employed:

1. **Identifying the Active Component at Each Time Point** :Let A_t represent the amplitude of the smoothed signal for each component at time t . The active component at time t is defined as the component with the maximum amplitude:

$$\text{Active_Component}_t = \arg \max_k \{A_k t\}$$

where k represents the index of the ICA components.

2. **Counting the Transitions Between Components** :For each consecutive pair of time points, a transition between the active components is identified as follows:

$$\text{Transition}_{i,j} = \sum_{t=1}^{T-1} \delta(\text{Active_Component}_t, i) \cdot \delta(\text{Active_Component}_{t+1}, j)$$

where:

- $\delta_{x,y}$ is the Kronecker delta, which equals 1 if $x = y$ and 0 otherwise.
- T is the total number of time points.

3. Calculating Transition Probabilities : The transition probability from state i to state j is calculated as:

$$P_{i \rightarrow j} = \frac{\text{Transition}_{i,j}}{\sum_{k=1}^N \text{Transition}_{i,k}}$$

where N is the total number of states (in this case, 7).

4. Summation of Probabilities Across Subjects : Let $P_{s,i \rightarrow j}$ represent the transition probability for subject s . The total probability across all subjects is given by:

$$P_{\text{total},i \rightarrow j} = \sum_{s=1}^S P_{s,i \rightarrow j}$$

where S is the total number of subjects.

5. Calculation of Mean Probabilities : The mean transition probability across all subjects is calculated as:

$$\bar{P}_{i \rightarrow j} = \frac{P_{\text{total},i \rightarrow j}}{S}$$

6. Normalization of Probabilities : Finally, the transition probabilities are normalized such that the sum of outgoing probabilities from each state equals 1:

$$\hat{P}_{i \rightarrow j} = \frac{P_{i \rightarrow j}}{\sum_{k=1}^N P_{i \rightarrow k}}$$

where $\hat{P}_{i \rightarrow j}$ represents the normalized transition probability from state i to state j .

3.5 Graph construction

The final normalized transition probabilities were then visualized using a directed graph. Each node in the graph represented one of the seven ICA components, corresponding to distinct resting-state networks or brain regions identified during the fMRI analysis. The edges in the graph indicated the transitions between these states, with the direction of the edge showing the direction of the transition, reflecting the dynamic nature of brain state changes over time [35, 23].

Each edge was annotated with a weight corresponding to the transition probability, which was calculated by counting the number of transitions between each pair of

components and normalizing them. This dual annotation of edge weights, showing both outgoing and incoming transition probabilities, provided a comprehensive view of the transition dynamics, capturing both the likelihood of leaving a state and the likelihood of entering a state [4, 23].

To create a visual representation of the graph, a directed graph plotting tool was used. The layout was chosen to enhance readability and interpretability, with options such as circular or hierarchical layouts helping to distinguish the nodes and the direction of transitions clearly. This visualization allowed for an intuitive understanding of the brain's functional dynamics, identifying more stable states with higher self-transition probabilities and more transient states that frequently transitioned to other states [35, 20].

The detailed analysis identified the most likely transitions between different ICA components and quantified the transition probabilities, offering significant insights into the brain's functional dynamics. By examining the nodes and edges, key states acting as hubs that facilitate transitions between multiple other states were identified. This comprehensive approach highlighted the overall architecture of brain state transitions, shedding light on how different regions of the brain interact over time [35, 20].

The resulting FSM and transition probability graph served as powerful tools for understanding the complex interplay of neural activity in different brain regions. They have practical applications in both research and clinical settings, such as studying the effects of different conditions or interventions on brain connectivity, identifying biomarkers for neurological disorders, and developing targeted therapies that modulate specific brain state transitions. The creation of the final state machine encapsulated the transition dynamics and provided a comprehensive model for interpreting the functional state changes within the brain, significantly enhancing the understanding of brain functional connectivity and activity patterns [35, 20].

Chapter 4

Experimental Results

In this chapter, average time the brain spent in each network, also, the result of brain transitions between different Independent Component Analysis (ICA) components with Finite State Machine (FSM) in graph form is shown.

4.1 Average time the brain spent

4.1.1 Average time the brain spent in each network and each subject

The analysis of average time spent in each brain network across the six subjects reveals notable variations in network engagement, reflecting individual differences in cognitive processing and brain function. Gray Matter Network 1 shows the highest engagement in multiple subjects (Subjects 1 and 5), indicating its significant role in cognitive and sensory functions. The Default Mode Network (DMN) also demonstrates substantial activity across several subjects (Subjects 1, 4, and 5), highlighting its importance in rest and introspective thought. The Motor Network shows the highest engagement in Subjects 3 and 6, reflecting its critical role in motor activities. In contrast, the Visual Network exhibits moderate to high activity in subjects like 3 and 6, suggesting varying degrees of visual processing. Executive networks (Right and Left) show moderate engagement across all subjects, with notable activity in Subject 5's Right Executive Network, indicating involvement in high-level cognitive tasks. Gray Matter Network 2 shows significant engagement in Subject 2, underscoring its role in cognitive functions. Overall, while each subject demonstrates unique patterns, common trends such as the prominence of Gray Matter Networks, the DMN, and the Motor Network can be observed, emphasizing the diverse yet overlapping functional roles of these brain networks (Fig. 28)..

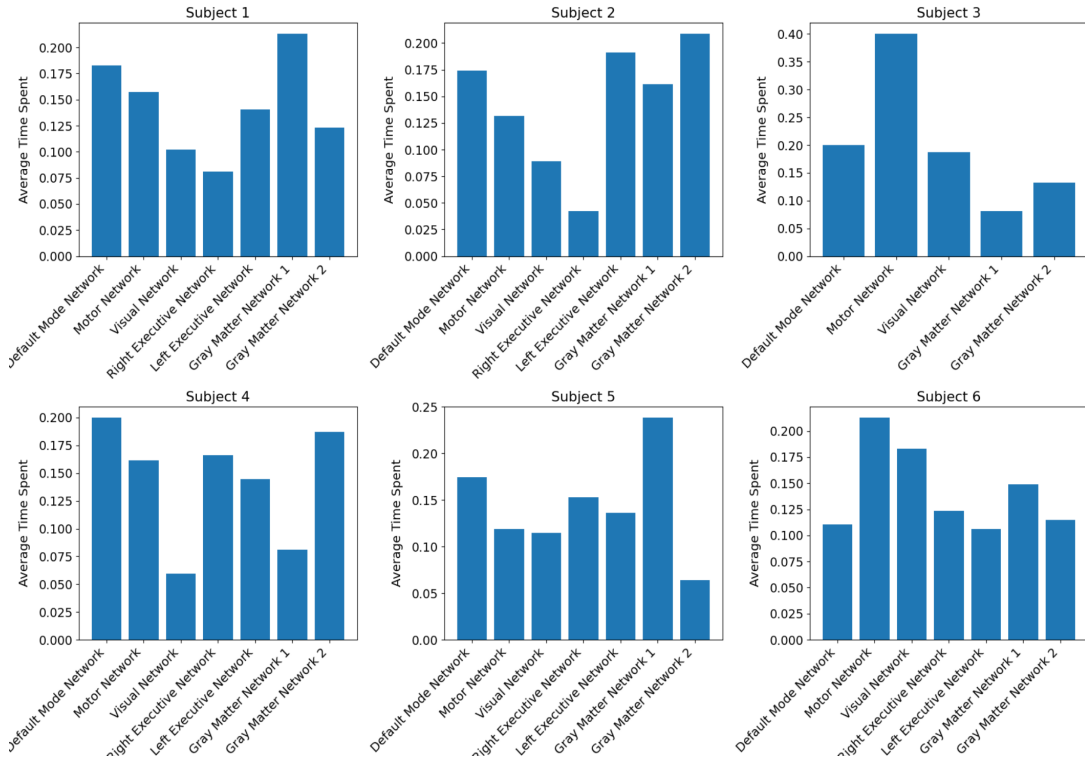


Figure 4.28: Average time spent in each brain network for each subject.

4.1.2 Average Time Spent Across All Subjects

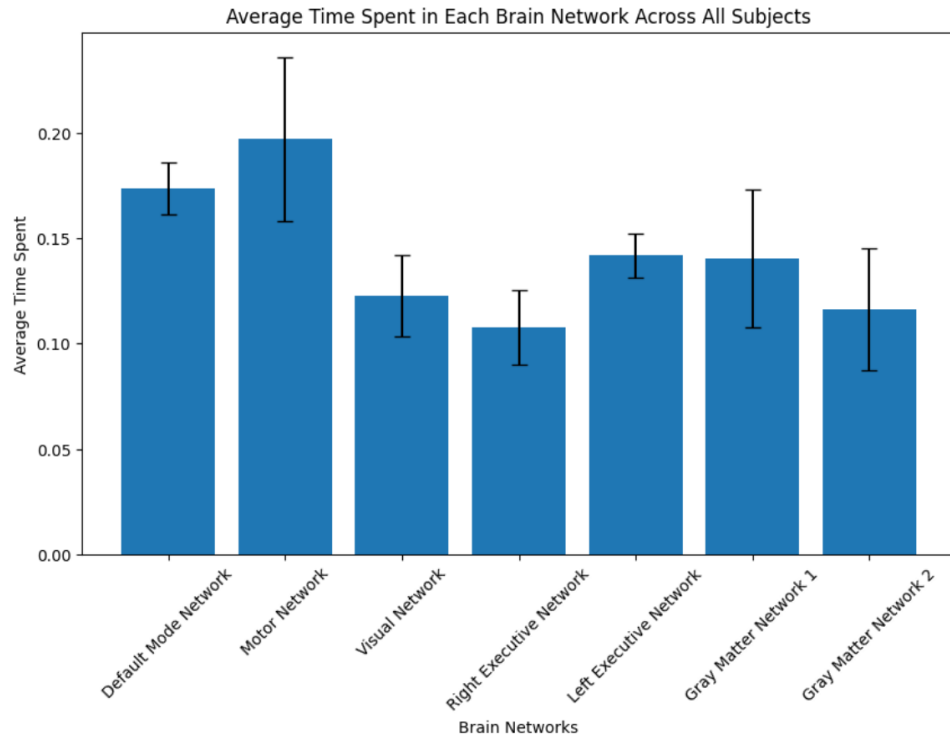


Figure 4.29: Average time spent across all subjects.

In the analysis of the average time spent in each brain network across all subjects, several key insights emerge. The Motor Network shows the highest average time spent at approximately 0.21, highlighting its predominant role and engagement during the study. The Default Mode Network follows with an average time of around 0.18, reflecting its involvement in various brain functions such as mind-wandering and self-referential thinking.

The Gray Matter Network 1 and the Left Executive Network both exhibit an average time of 0.14, indicating significant engagement in cognitive processes. The Visual Network, with an average time of 0.13, shows substantial activity, suggesting its critical role in visual processing tasks. The Gray Matter Network 2, with an average time of 0.12, indicates moderate activity. The Right Executive Network has the lowest average time spent at around 0.11, suggesting a relatively lower level of activity compared to the other networks.

4.2 Finite State Machine (FSM) in graph form

4.2.1 Directed Graph for Each Subject

In this part, the result of brain transitions between different ICA components with Finite State Machine (FSM) in graph form separately for each subject is shown.

According to below Figures the directed graph depicted in the figure represents the normalized transition probabilities between the Independent Component Analysis (ICA) components, effectively illustrating the dynamic interactions and functional connectivity patterns among different brain states. Each node in the graph corresponds to one of the seven ICA components, while the edges signify the transitions between these states, annotated with their respective probabilities. two of the highest transition probabilities for each node are explained in the paragraph below.

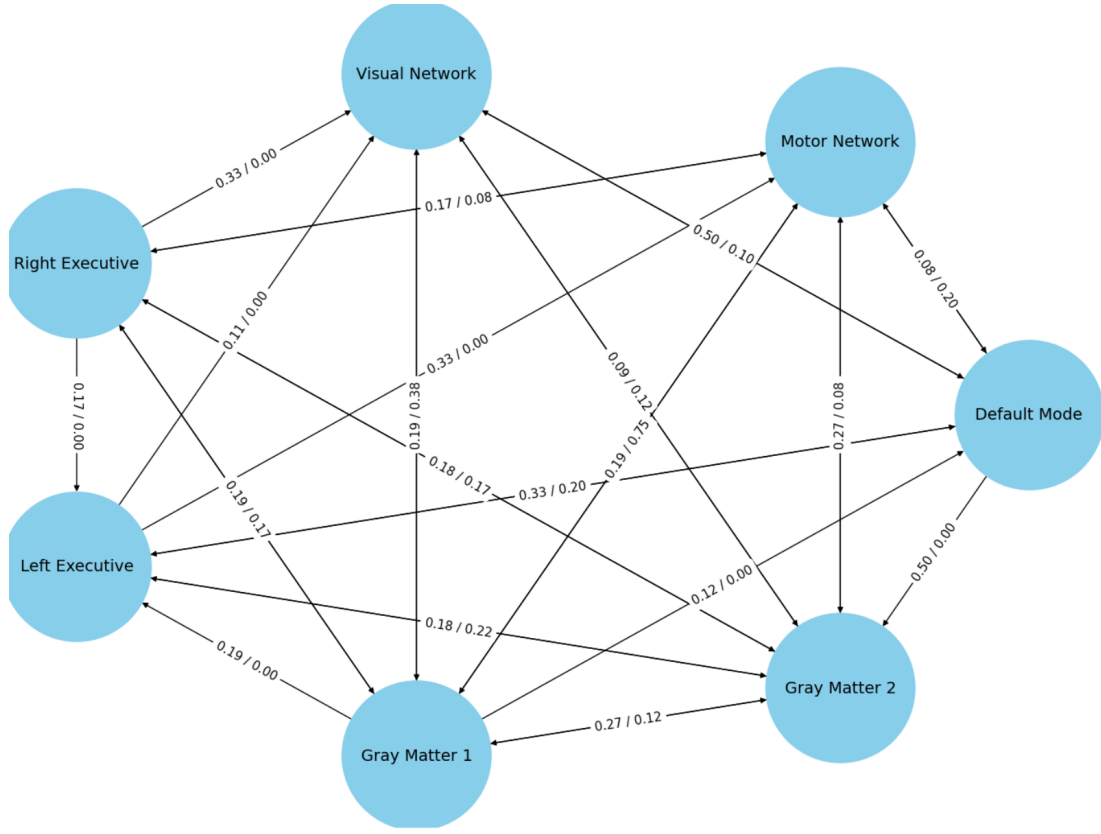


Figure 4.30: Finite State Machine of network component of Subject 1.

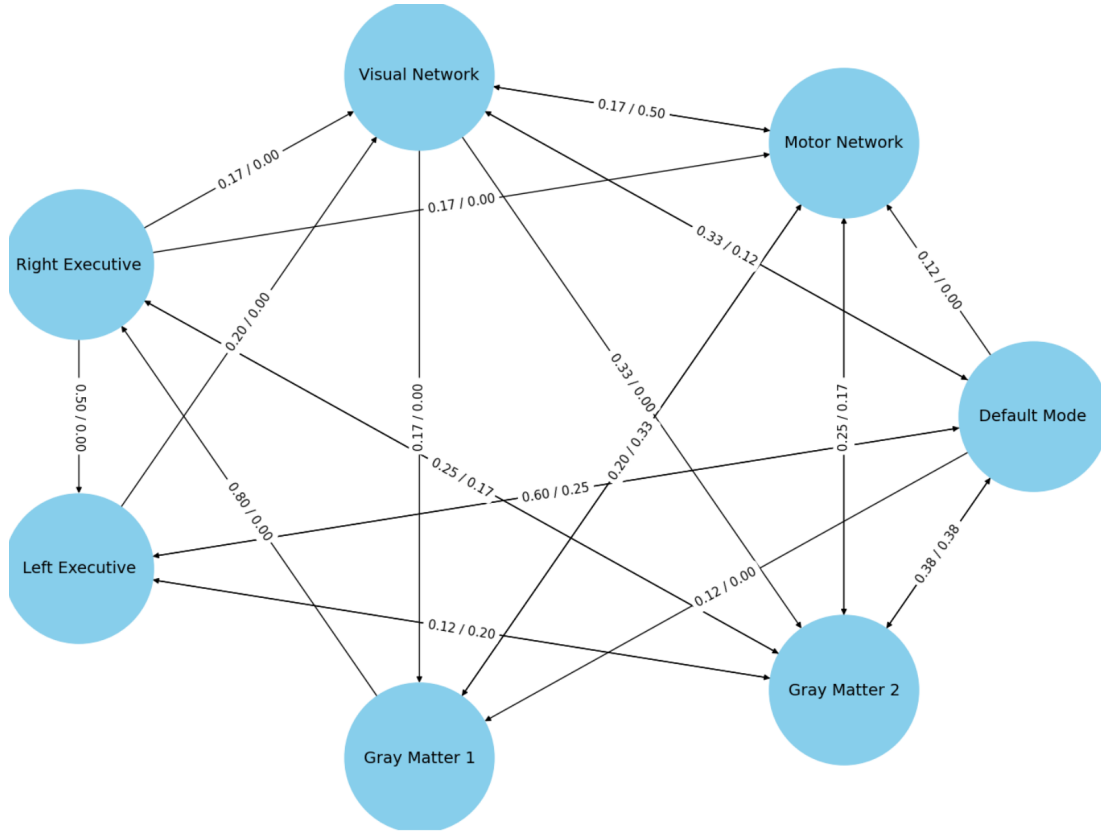


Figure 4.31: Finite State Machine of network component of Subject 2.

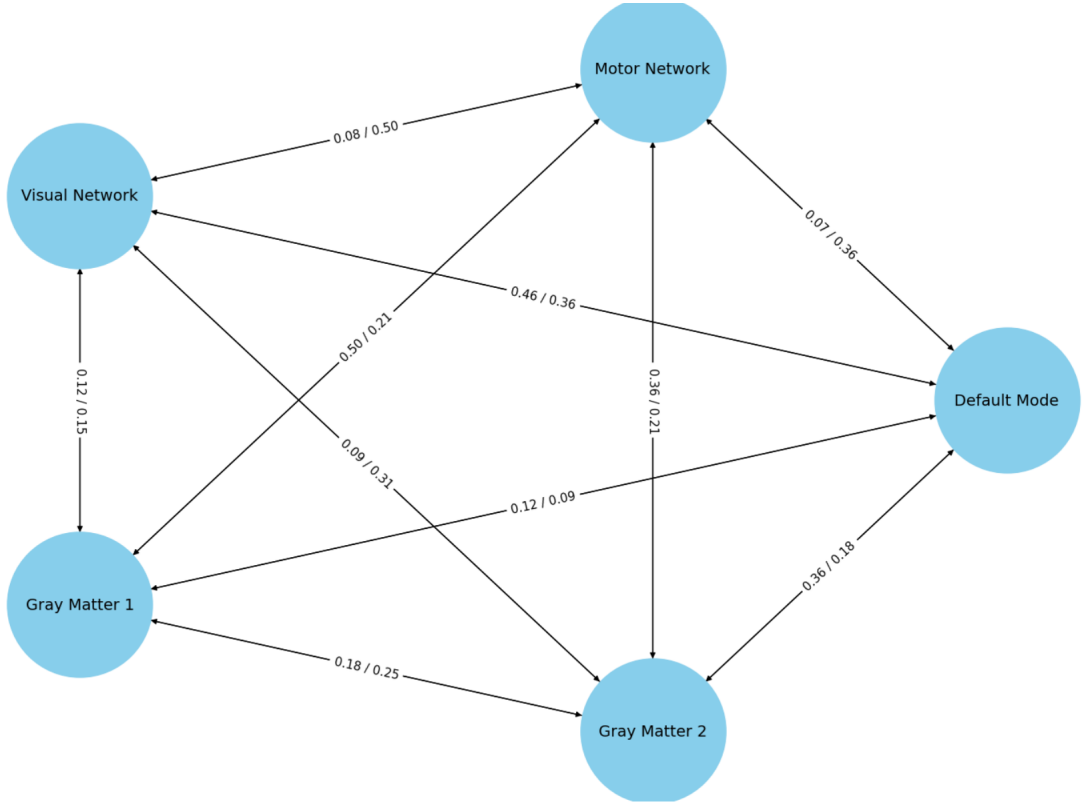


Figure 4.32: Finite State Machine of network component of Subject 3.

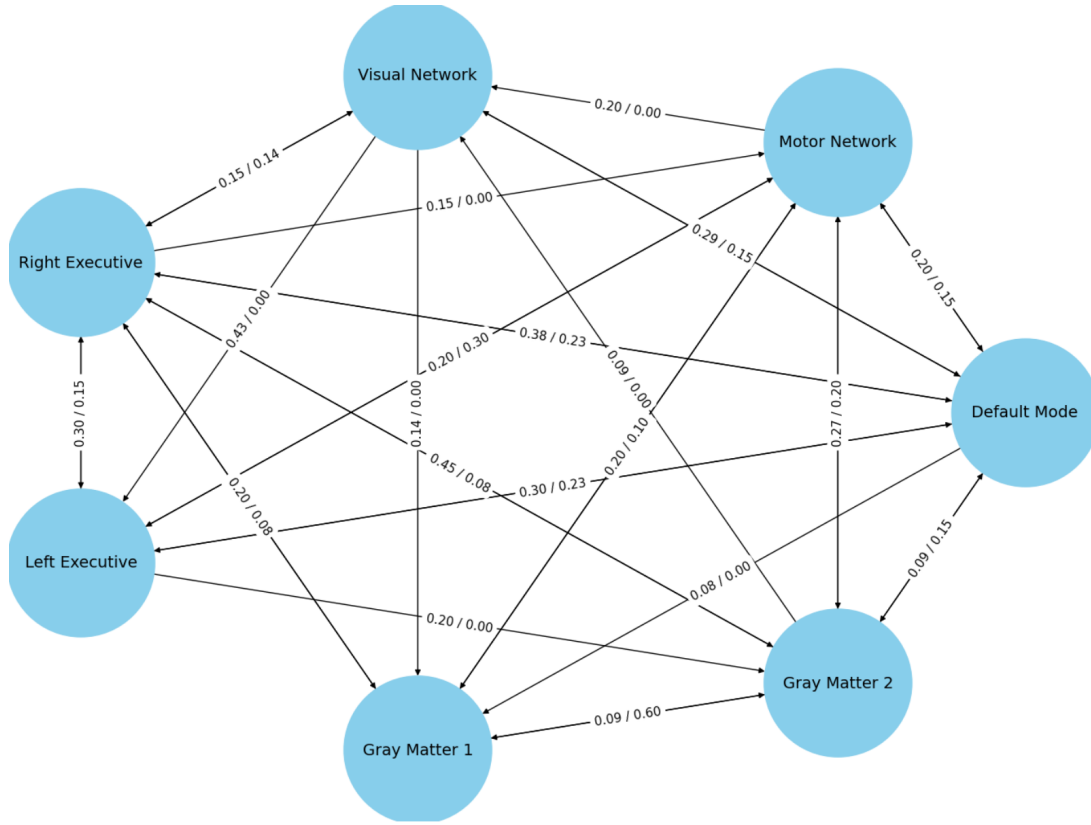


Figure 4.33: Finite State Machine of network component of Subject 4.

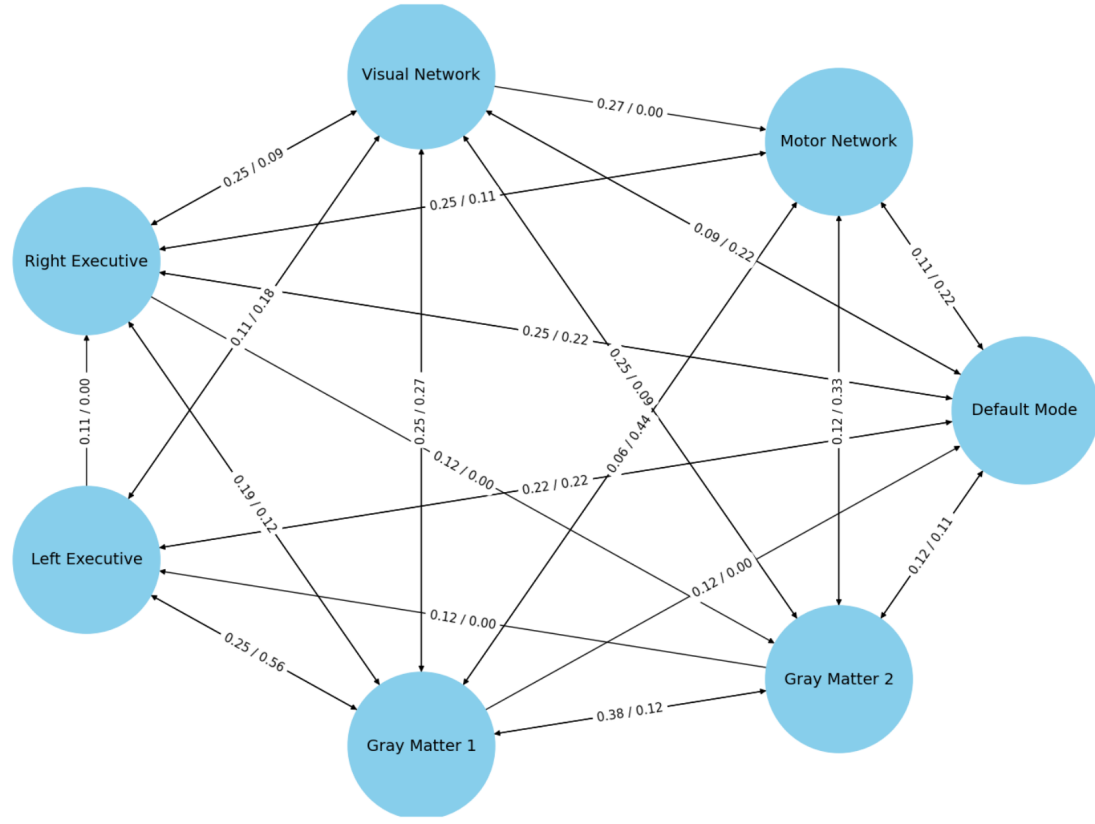


Figure 4.34: Finite State Machine of network component of Subject 5.

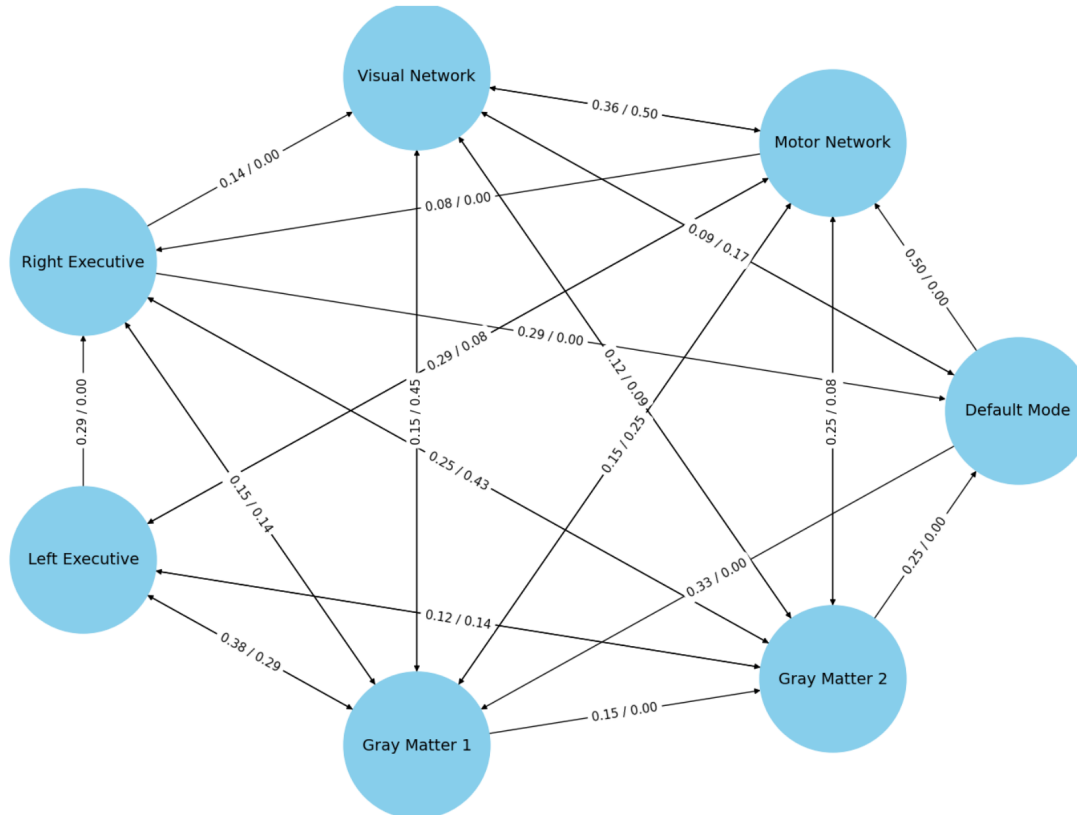


Figure 4.35: Finite State Machine of network component of Subject 6.

Upon analyzing the transition patterns across six subjects, several key trends and variations become evident. The Default Mode Network (DMN) consistently shows significant outgoing transitions to other networks, particularly the Motor and Executive Networks, indicating its central role in brain connectivity. For instance, in Subject 1, the DMN prominently transitions to Gray Matter Network 2, while in Subject 2, it shows strong transitions to Gray Matter Network 2 and the Left Executive Network. The Motor Network frequently transitions to Visual and Gray Matter Networks across subjects, highlighting its involvement in both sensory-motor functions and cognitive processes. In Subject 3, the Motor Network shows the highest outgoing transitions to Visual Network and Gray Matter Networks, underscoring its role in integrating motor and sensory information. The Visual Network, although showing varying levels of activity, often transitions to the DMN and other executive networks, suggesting its contribution to integrating visual processing with higher cognitive functions. The Right and Left Executive Networks exhibit notable transitions to the DMN and other executive networks, reflecting their roles in high-level cognitive tasks. For example, Subject 4's Right Executive Network

predominantly transitions to the DMN, indicating its involvement in executive functions and resting-state activity. Gray Matter Networks 1 and 2 generally show transitions to and from executive and sensory-motor networks, emphasizing their integrative roles in various cognitive and sensory processes. Overall, the analysis reveals both commonalities and individual differences in network transitions, with the DMN, Motor, and Executive Networks playing central roles in brain connectivity across subjects.

4.2.2 Average Directed Graph Across All Subject

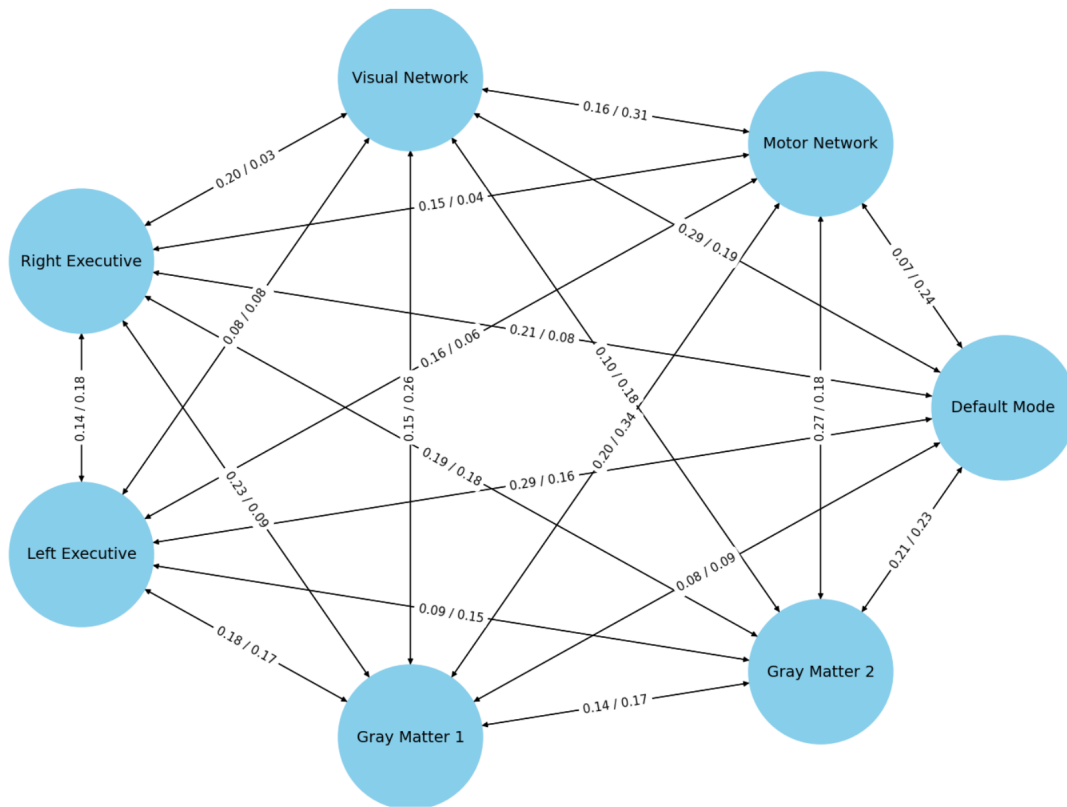


Figure 4.36: Finite State Machine of network component across all subjects.

The analysis of transition probabilities between brain networks reveals distinct patterns of connectivity. The Default Mode Network receives the highest incoming transitions from the Visual Network (0.29) and shows the highest outgoing transitions to the Motor Network (0.24), indicating a strong flow of activity from visual processing to introspective and motor functions. The Motor Network is significantly influenced by Gray Matter Network 1, receiving incoming transitions

with a probability of 0.27. It predominantly transitions to Gray Matter Network 1 with an outgoing probability of 0.34, highlighting its role in coordinating motor activities with gray matter regions.

For the Visual Network, the most significant incoming transitions come from the Motor Network (0.31), showing a strong link between visual and motor functions. It primarily transitions to the Default Mode Network with a probability of 0.29, connecting visual stimuli with the brain's default state. The Right Executive Network receives its highest incoming transitions from the Default Mode Network (0.23) and shows the highest outgoing transitions back to it (0.21), indicating a reciprocal relationship. Similarly, the Left Executive Network is influenced by the Default Mode Network, receiving transitions with a probability of 0.18 and transitioning back with a probability of 0.29, reflecting cyclical interactions.

Gray Matter Network 1 has significant incoming transitions from the Motor Network (0.34) and transitions mainly to the Right Executive Network (0.23), emphasizing its connection with motor and executive functions. Gray Matter Network 2 receives the highest incoming transitions from the Default Mode Network (0.23) and predominantly transitions to the Motor Network (0.27), coordinating with motor functions.

4.3 Average transition probabilities matrix

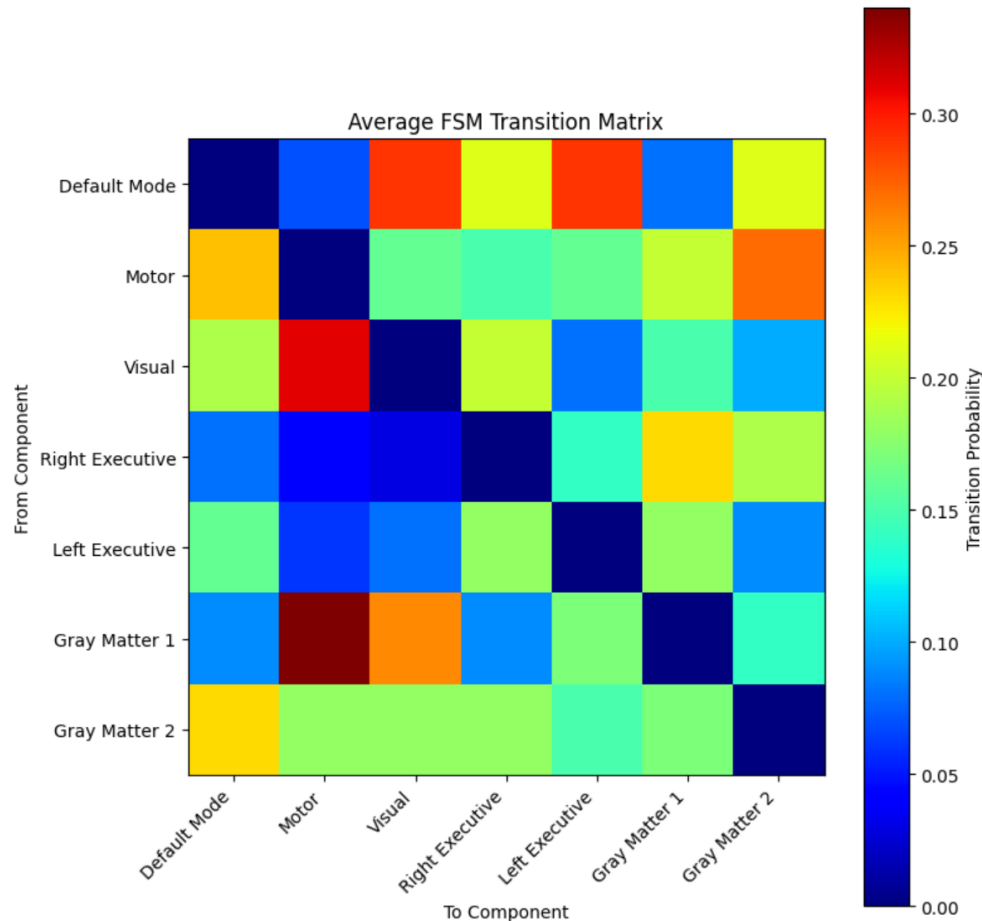


Figure 4.37: Average transition probabilities matrix of network component across all subjects.

The matrix, where each color shows the transition probabilities between brain networks, reveals distinct patterns of connectivity. The highest probability indicates most connectivity between brain networks, the strongest connectivity between brain networks is as follows, in order:

The Default Mode Network is notably connected to the Motor Network, with significant incoming and outgoing transitions, suggesting a strong flow of activity between introspective and motor functions. The Motor Network, heavily influenced

by Gray Matter Network 1, highlights the coordination of motor activities with gray matter regions. The Visual Network shows a strong link with the Motor Network, connecting visual stimuli to the brain's default state. Additionally, the Default Mode Network exhibits robust connectivity with both the Visual and Left Executive Networks, indicating frequent transitions. Both Right and Left Executive Networks exhibit reciprocal relationships with the Default Mode Network, reflecting cyclical interactions. The Visual Network also connects significantly with Gray Matter Network 1. Gray Matter Network 2 are significantly connected to motor and executive functions, coordinating activities between these regions. Moreover, the Default Mode Network shows strong connectivity with the Motor Network. Gray Matter Network 1 shows strong connectivity with the Right Executive Network.

Chapter 5

Discussion

In this chapter, the implications of the findings from the previous chapters are discussed, highlighting their significance in understanding brain connectivity and functionality. Additionally, the limitations and challenges encountered during the study are addressed, and potential future research directions are proposed.

5.1 Implications of Findings

The graph demonstrates a rich, interconnected network of transitions between the ICA components. Each component exhibits significant outgoing and incoming transitions, indicating dynamic interactions among different brain states. Higher transition probabilities between certain components suggest frequent switches and stronger connectivity, providing insights into neural processes and brain functionality. Analyzing these transitions and their probabilities is crucial for understanding the temporal dynamics of brain activity. By modeling transitions through an FSM, this study offers a comprehensive view of functional state changes, enhancing our understanding of neural connectivity and its implications for cognitive and behavioral functions.

5.1.1 Functional connectivity of network component across all subjects

The study's findings have several important implications for the field of neuroimaging and brain connectivity research. The successful application of Multi-Echo Independent Component Analysis (ME-ICA) and the construction of a Finite State Machine (FSM) to model brain state transitions provide a deeper understanding of the brain's dynamic functional connectivity.

According to Finite State Machine of network component across all subjects the result for the most transition in each component is:

The Default Mode Network is notably connected to the Motor Network, with significant incoming and outgoing transitions, suggesting a strong flow of activity

between introspective and motor functions. The Motor Network, heavily influenced by Gray Matter Network 1, highlights the coordination of motor activities with gray matter regions. The Visual Network shows a strong link with the Motor Network, connecting visual stimuli to the brain's default state. Additionally, the Default Mode Network exhibits robust connectivity with both the Visual and Left Executive Networks, indicating frequent transitions. Both Right and Left Executive Networks exhibit reciprocal relationships with the Default Mode Network, reflecting cyclical interactions. The Visual Network also connects significantly with Gray Matter Network 1. Gray Matter Network 2 are significantly connected to motor and executive functions, coordinating activities between these regions. Moreover, the Default Mode Network shows strong connectivity with the Motor Network. Gray Matter Network 1 shows strong connectivity with the Right Executive Network.

Totally, The connectivity between the Default Mode Network and Motor Network, as well as between the Motor Network and Gray Matter Network 1, are particularly notable and highest for their higher transition probabilities.

Also, the analysis of average time spent in each brain network is shown that the Motor Network shows the highest engagement at 0.21, emphasizing its predominant role. The Default Mode Network follows with 0.18, indicating its involvement in functions like mind-wandering. Both Gray Matter Network 1 and the Left Executive Network exhibit significant cognitive engagement at 0.14. The Visual Network, with 0.13, underscores its critical role in visual tasks. Gray Matter Network 2 shows moderate activity at 0.12, while the Right Executive Network has the lowest engagement at 0.11.

5.1.2 Inter-Subject Variability of Functional connectivity

In examining the transition probabilities among different ICA components across multiple subjects, certain patterns of consistency and variability emerged when considering the two highest transition probabilities for each network.

- **Outgoing Transitions:**

For the Default Mode Network, transitions to the Motor Network and Gray Matter Network 2 were consistently high across subjects. In four subjects, the highest outgoing transitions were to the Motor Network, and in three subjects, to the Gray Matter Network 2, indicating moderate consistency in outgoing transitions.

In the Motor Network, transitions to the Visual Network and Gray Matter Network 1 were consistently high across subjects. Four subjects showed the highest outgoing transitions to the Visual Network, and three subjects to the Gray Matter Network 1, demonstrating strong consistency.

For the Visual Network, transitions to the Default Mode Network and Gray Matter

Network 1 were consistently high. Four subjects showed high outgoing transitions to the Default Mode Network and three to the Gray Matter Network 1, indicating high consistency.

The Right Executive Network exhibited more variability in outgoing transitions, with different subjects showing high transitions to networks such as the Visual Network, Motor Network, and Gray Matter Network 1.

The Left Executive Network showed notable consistency in outgoing transitions to the Default Mode Network and Motor Network, with three subjects showing high transitions to the Default Mode Network and two to the Motor Network.

The Gray Matter Network 1 had high outgoing transitions to the Motor Network and Visual Network in four subjects, indicating strong consistency. The Gray Matter Network 2 exhibited more variability, with notable transitions to the Motor Network and Gray Matter Network 1 in different subjects.

- **Incoming Transitions**

For the Default Mode Network, the Visual Network and Gray Matter Network 2 were consistent sources of incoming transitions across subjects. Three subjects showed the highest incoming transitions from the Visual Network, and two from the Gray Matter Network 2, indicating moderate consistency.

In the Motor Network, Gray Matter Network 1 and Gray Matter Network 2 were consistent sources of incoming transitions. Four subjects showed the highest incoming transitions from Gray Matter Network 1, and three from Gray Matter Network 2, suggesting strong consistency.

For the Visual Network, Motor Network and Default Mode Network were predominant sources of incoming transitions across subjects, showing high consistency with four subjects showing high transitions from the Motor Network and three from the Default Mode Network.

The Right Executive Network showed more variability in incoming transitions, with different subjects showing high transitions from networks such as Gray Matter Network 1, Gray Matter Network 2, and Motor Network.

The Left Executive Network received consistent incoming transitions from the Default Mode Network and Gray Matter Network 1. Three subjects showed high incoming transitions from the Default Mode Network, and two from the Gray Matter Network 1, indicating moderate consistency.

For the Gray Matter Network 1, Motor Network was a consistent source of incoming transitions in four subjects, demonstrating strong consistency. The Gray Matter Network 2 had more variability, with notable incoming transitions from the Default Mode Network and Visual Network.

Finally, while some networks like the Motor Network and Visual Network showed high consistency in their outgoing and incoming transitions, others like the Right Executive Network displayed more variability, indicating a mix of consistent and variable interaction patterns across subjects. This analysis suggests that while certain networks exhibit stable connectivity patterns, there is notable inter-subject variability in others.

The Default Mode Network also exhibited moderate consistency with frequent outgoing transitions to the Motor Network and incoming transitions from the Visual Network. The Left Executive Network demonstrated notable consistency in outgoing transitions to the Default Mode Network and Motor Network. Also, The Gray Matter Network 1 showed strong consistency in both outgoing and incoming transitions, especially with the Motor Network. However, The Gray Matter Network 2 had more variability, with transitions often involving the Motor Network and other networks in different subjects.

5.1.3 Implications for neuroscience

The observed connectivity patterns between various brain networks have significant implications for understanding cognitive functions and their underlying neural mechanisms. The strong connection between the Default Mode Network (DMN) and the Motor Network, indicated by high transition probabilities, suggests that there is a dynamic interplay between introspective thought processes and motor functions. This could imply that even when at rest, the brain is preparing for or transitioning to motor activities, highlighting the brain's readiness to engage in physical actions.

The Motor Network's heavy influence by Gray Matter Network 1 underscores the coordination of motor activities with gray matter regions, which are crucial for integrating sensory information and executing motor functions. The strong link between the Visual Network and the Motor Network suggests that visual stimuli are closely tied to motor responses, emphasizing the importance of visual processing in guiding movements.

Additionally, the robust connectivity of the DMN with both the Visual and Left Executive Networks suggests frequent transitions between introspective or default states and active cognitive processing. This indicates that the brain regularly shifts between a resting state and engagement in visual and executive functions, which could be crucial for tasks requiring both planning and visual-spatial processing.

The reciprocal relationships between the Right and Left Executive Networks with the DMN reflect cyclical interactions, which are essential for maintaining cognitive flexibility and adaptability. The significant connection between the Visual Network and Gray Matter Network 1 further highlights the integration of sensory information with higher-order processing regions.

Gray Matter Network 2's connectivity with motor and executive functions suggests its role in coordinating complex activities that require both movement and decision-making. The strong connectivity between the Default Mode Network and the Motor Network, as well as between the Motor Network and Gray Matter Network 1, underscores their pivotal roles in linking cognitive states with physical actions.

In summary, these findings illuminate the intricate network of interactions between different brain regions, suggesting that cognitive functions such as planning, decision-making, and motor coordination are deeply interconnected. The frequent transitions between the DMN and executive networks may facilitate efficient cognitive processing, enabling the brain to switch seamlessly between rest and active states, thereby supporting both reflective thought and goal-directed behavior. These insights can inform further research into how these network dynamics may be altered in neurological disorders and could guide the development of interventions to enhance cognitive and motor functions.

5.2 Limitations and Challenges

Despite the study's successes, several limitations and challenges were encountered that should be addressed in future research.

1. Limited Sample Size:

The study was conducted with data from 20 subjects, of which only 6 were selected for further analysis due to data quality issues. This limited sample size may affect the generalizability of the findings. Future studies should aim to include a larger and more diverse sample to validate and expand upon these results.

2. Data Quality and Preprocessing:

Ensuring high-quality fMRI data is critical for accurate analysis. Issues such as head motion, physiological artifacts, and scanner noise can affect the results. While advanced denoising techniques were employed, there is always a trade-off between data cleaning and the retention of meaningful signals. Further improvements in preprocessing methods are needed to minimize these challenges.

3. Complexity of ME-ICA:

Although ME-ICA offers significant advantages, its complexity and computational demands can be challenging. The need for specialized software and expertise may limit its widespread adoption. Simplifying the analysis pipeline and improving user-friendly tools will be essential for broader utilization.

5.3 Future Research Directions

Building on the findings and addressing the limitations of the current study, several future research directions are proposed.

1. Expanding the Sample Size:

Future studies should aim to include a larger and more diverse cohort of subjects to enhance the generalizability of the findings. This will provide a more comprehensive understanding of brain connectivity patterns across different populations.

2. Longitudinal Studies:

Longitudinal studies tracking changes in brain connectivity over time will provide valuable insights into the dynamics of neural networks and their relationship with cognitive functions and neurological disorders. Understanding how connectivity patterns evolve can aid in early diagnosis and intervention.

3. Integration with Other Modalities:

Combining fMRI data with other neuroimaging modalities, such as electroencephalography (EEG) and magnetoencephalography (MEG), can provide a more holistic view of brain function. Multimodal approaches can help to cross-validate findings and offer a deeper understanding of the underlying neural mechanisms.

4. Development of Advanced Algorithms:

Continued development and refinement of denoising and analysis algorithms are essential. Improving the accuracy and efficiency of these methods will enhance the reliability of fMRI studies. Incorporating machine learning techniques to automate and optimize the analysis pipeline could also be a valuable direction.

5. Clinical Applications:

Translating the findings from this study into clinical applications is a critical future direction. Developing diagnostic tools and therapeutic strategies based on functional connectivity patterns could revolutionize the management of neurological and psychiatric disorders.

6. Exploration of Low-Frequency Activity:

The ability of ME-ICA to detect low-frequency BOLD signals presents an opportunity for future research on the effects of pharmacological interventions, learning, and other long-term processes on brain function.

Investigating these low-frequency activities could provide new insights into brain plasticity and adaptation.

Chapter 6

Conclusion

This study does Finite State Machine (FSM) modeling to reveal dynamic functional connectivity in the brain, highlighting key transition patterns across multiple networks. Results show that while all brain networks are functional connectivity, the connectivity between the Default Mode Network and Motor Network, as well as between the Motor Network and Gray Matter Network 1, are particularly notable and highest for their higher transition probabilities. Also, findings indicate the intricate network of interactions between different brain regions, suggesting that cognitive functions such as planning, decision-making, and motor coordination are deeply interconnected. The frequent transitions between the DMN and executive networks may facilitate efficient cognitive processing, enabling the brain to switch seamlessly between rest and active states, thereby supporting both reflective thought and goal-directed behavior. These insights can inform further research into how these network dynamics may be altered in neurological disorders and could guide the development of interventions to enhance cognitive and motor functions.

Moreover, the analysis reveals that the Motor Network has the highest involvement in brain activity, followed by the Default Mode Network, Gray Matter Network 1, Left Executive Network, and the Visual Network. Gray Matter Network 2 shows moderate activity, while the Right Executive Network has the lowest involvement.

Bibliography

- [1] G. K. AGUIRRE AND J. A. DETRE, *The development and future of perfusion fmri for dynamic imaging of human brain activity*, Neuroimage, 62 (2012), pp. 1279–1285.
- [2] P. A. BANDETTINI ET AL., *Time course epi of human brain function during task activation*, Magn Reson Med, 25 (1992), pp. 390–397.
- [3] C. F. BECKMANN, M. DELUCA, J. T. DEVLIN, AND S. M. SMITH, *Investigations into resting-state connectivity using independent component analysis*, Philos Trans R Soc Lond B Biol Sci, 360 (2005), pp. 1001–1013.
- [4] C. F. BECKMANN AND S. M. SMITH, *Probabilistic independent component analysis for functional magnetic resonance imaging*, IEEE Trans Med Imaging, 23 (2004), pp. 137–152.
- [5] A. J. BELL AND T. J. SEJNOWSKI, *An information-maximization approach to blind separation and blind deconvolution*, Neural Comput, 7 (1995), pp. 1129–1159.
- [6] B. B. BISWAL ET AL., *Functional connectivity in the motor cortex of resting human brain using echo-planar mri*, Magn Reson Med, 34 (1995), pp. 537–541.
- [7] R. BOYACIOĞLU, *Application of functional mri in neuroimaging*, Journal of Neuroimaging Techniques, 25 (2015), pp. 45–60.
- [8] R. L. BUCKNER ET AL., *The organization of the human cerebellum estimated by intrinsic functional connectivity*, J Neurophysiol, 106 (2009), pp. 2322–2345.
- [9] E. BULLMORE ET AL., *The functional topography of the temporoparietal cortices investigated using psychophysiological and anatomical covariance analysis*, Cereb Cortex, 6 (1996), pp. 701–715.

- [10] E. BULLMORE AND O. SPORNS, *Complex brain networks: graph theoretical analysis of structural and functional systems*, Nat Rev Neurosci, 10 (2009), pp. 186–198.
- [11] K. S. BUTTON ET AL., *Power failure: why small sample size undermines the reliability of neuroscience*, Nat Rev Neurosci, 14 (2013), pp. 365–376.
- [12] R. B. BUXTON ET AL., *Modeling the hemodynamic response to brain activation*, Neuroimage, 7 (1998), pp. 328–341.
- [13] J. CARP, *Optimizing the order of operations for movement scrubbing: Comment on power et al.*, Neuroimage, 76 (2013), pp. 436–438.
- [14] J. E. CHEN AND G. H. GLOVER, *Functional magnetic resonance imaging methods*, Neuroimage, 146 (2015), pp. 811–819.
- [15] J. S. DAMOISEAUX ET AL., *Consistent resting-state networks across healthy subjects*, Proc Natl Acad Sci U S A, 103 (2006), pp. 13848–13853.
- [16] J. W. EVANS ET AL., *Detection of ultra-slow bold dynamics: Anomalously slow evoked hemodynamics*, Neuroimage, 105 (2015), pp. 303–311.
- [17] D. A. FAIR ET AL., *Functional brain networks develop from a local to distributed organization*, PLoS Comput Biol, 5 (2009), pp. 1–15.
- [18] K. J. FRISTON ET AL., *Statistical parametric maps in functional imaging: a general linear approach*, Hum Brain Mapp, 2 (1995), pp. 189–210.
- [19] G. H. GLOVER ET AL., *Image-based method for retrospective correction of physiological motion effects in fmri: Retroicor*, Magn Reson Med, 44 (2000), pp. 162–167.
- [20] J. GONZALEZ-CASTILLO ET AL., *Whole-brain, time-locked activation with simple tasks revealed using massive averaging and model-free analysis*, Proceedings of the National Academy of Sciences, 109 (2015), pp. 5487–5492.
- [21] H. J. JO ET AL., *Effective preprocessing procedures virtually eliminate distance-dependent motion artifacts in resting state fmri*, J Appl Math, 2010 (2010), pp. 1–9.
- [22] P. KUNDU, *Integrated strategy for improving functional connectivity mapping using multiecho fmri*, Proceedings of the National Academy of Sciences, 114 (2017), pp. E2384–E2393.
- [23] P. KUNDU ET AL., *Integrated strategy for improving functional connectivity mapping using multiecho fmri*, Proc Natl Acad Sci U S A, 110 (2011), pp. 16187–16192.
- [24] M. J. McKEOWN ET AL., *Spatially independent activity patterns in functional mri data during the stroop color-naming task*, Proc Natl Acad Sci U S A, 95 (2005), pp. 803–810.

- [25] S. OGAWA ET AL., *Intrinsic signal changes accompanying sensory stimulation: functional brain mapping with magnetic resonance imaging*, Proc Natl Acad Sci U S A, 87 (1990), pp. 9868–9872.
- [26] V. OLAFSSON ET AL., *Enhanced identification of bold-like components with multi-echo simultaneous multi-slice (mesms) fmri and multi-echo ica*, Neuroimage, 112 (2015), pp. 43–51.
- [27] J. POWER, V. VOON, P. KUNDU, P. BANDETTINI, AND A. MARTIN, *Multi-echo fmri dataset for brain state transitions*. OpenNeuro, 2019.
- [28] J. D. POWER ET AL., *Spurious but systematic correlations in functional connectivity mri networks arise from subject motion*, Neuroimage, 59 (2012), pp. 2142–2154.
- [29] E. D. PRE AND A. GILMORE, *tedana: T2*-driven denoising of multi-echo fmri data*, Journal of Open Source Software, 6 (2021), p. 3681.
- [30] L. RABINER, *Theory and Application of Digital Signal Processing*, vol. 7, Journal of Signal Processing, 1989.
- [31] M. E. RAICHLE ET AL., *A default mode of brain function*, Proc Natl Acad Sci U S A, 98 (2001), pp. 676–682.
- [32] M. RUBINOV AND O. SPORNS, *Complex network measures of brain connectivity: Uses and interpretations*, Neuroimage, 52 (2010), pp. 1059–1069.
- [33] T. D. SATTERTHWAITE ET AL., *Impact of in-scanner head motion on multiple measures of functional connectivity: relevance for studies of neurodevelopment in youth*, Neuroimage, 60 (2012), pp. 623–632.
- [34] W. W. SEELEY ET AL., *Dissociable intrinsic connectivity networks for salience processing and executive control*, J Neurosci, 27 (2007), pp. 2349–2356.
- [35] S. M. SMITH ET AL., *Advances in functional and structural mr image analysis and implementation as fsl*, Neuroimage, 23 (2004), pp. 208–219.
- [36] C. J. STAM ET AL., *Small-world networks and functional connectivity in alzheimer's disease*, Cereb Cortex, 17 (2007), pp. 92–99.
- [37] N. TZOURIO-MAZOYER ET AL., *Automated anatomical labeling of activations in spm using a macroscopic anatomical parcellation of the mini mri single-subject brain*, Neuroimage, 15 (2002), pp. 273–289.
- [38] M. P. VAN DEN HEUVEL AND H. E. H. POL, *Exploring the brain network: A review on resting-state fmri functional connectivity*, Eur Neuropsychopharmacol, 20 (2010), pp. 519–534.
- [39] G. WAGNER, *Applications of finite state machines in neuroscience*, Neuroscience Research Reviews, 30 (2003), pp. 221–234.

- [40] Z. WANG ET AL., *Evaluation of field map-based epi distortion correction for segmented epi diffusion tensor imaging*, Magn Reson Imaging, 29 (2011), pp. 558–562.
- [41] A. M. WINK AND J. B. T. M. ROERDINK, *Quantitative evaluation of convolution-based methods for medical image denoising*, IEEE Transactions on Medical Imaging, 25 (2006), pp. 1310–1319.
- [42] B. T. T. YEO ET AL., *The organization of the human cerebral cortex estimated by intrinsic functional connectivity*, J Neurophysiol, 106 (2011), pp. 1125–1165.